



The effect of GCM biases on global runoff simulations of a land surface model

Lamprini V. Papadimitriou¹, Aristeidis G. Koutroulis¹, Manolis G. Grillakis¹, and Ioannis K. Tsanis^{1,2}

¹Technical University of Crete, School of Environmental Engineering, Chania, Greece

²McMaster University, Department of Civil Engineering, Hamilton, ON, Canada

Correspondence to: Ioannis K. Tsanis (tsanis@hydromech.gr)

Received: 7 April 2017 – Discussion started: 19 April 2017

Revised: 10 July 2017 – Accepted: 28 July 2017 – Published: 7 September 2017

Abstract. Global climate model (GCM) outputs feature systematic biases that render them unsuitable for direct use by impact models, especially for hydrological studies. To deal with this issue, many bias correction techniques have been developed to adjust the modelled variables against observations, focusing mainly on precipitation and temperature. However, most state-of-the-art hydrological models require more forcing variables, in addition to precipitation and temperature, such as radiation, humidity, air pressure, and wind speed. The biases in these additional variables can hinder hydrological simulations, but the effect of the bias of each variable is unexplored. Here we examine the effect of GCM biases on historical runoff simulations for each forcing variable individually, using the JULES land surface model set up at the global scale. Based on the quantified effect, we assess which variables should be included in bias correction procedures. To this end, a partial correction bias assessment experiment is conducted, to test the effect of the biases of six climate variables from a set of three GCMs. The effect of the bias of each climate variable individually is quantified by comparing the changes in simulated runoff that correspond to the bias of each tested variable. A methodology for the classification of the effect of biases in four effect categories (ECs), based on the magnitude and sensitivity of runoff changes, is developed and applied. Our results show that, while globally the largest changes in modelled runoff are caused by precipitation and temperature biases, there are regions where runoff is substantially affected by and/or more sensitive to radiation and humidity. Global maps of bias ECs reveal the regions mostly affected by the bias of each variable. Based on our findings, for global-scale applications, bias correction of radiation and humidity, in addition to that of precipitation

and temperature, is advised. Finer spatial-scale information is also provided, to suggest bias correction of variables beyond precipitation and temperature for regional studies.

1 Introduction

In recent years, there has been a strong consensus on the changes in climate caused by increased concentrations of anthropogenic greenhouse gas emissions (King et al., 2015; O’Neill et al., 2017; Stocker et al., 2013). Under the pressing circumstances of a warming world, scientific research has focused on estimating the range of changes in the future climate and the effectiveness of different adaptation strategies. The main tool for the investigation of future climate is the utilization of global climate models (GCMs). GCMs are based on physical principles that describe the components of the climate system, such as cloud formation and water and energy flux exchanges.

Although each generation of GCMs shows improvements compared to its predecessor (Koutroulis et al., 2016), climate model outputs still contain substantial biases that are expressed as deviations of the modelled climate variables from respective historical observations. These inherent biases can emanate from misrepresentations of physical atmospheric processes (Maraun, 2012), from uncertainties regarding the boundary and initial model conditions (Bromwich et al., 2013), and from the relatively coarse resolution employed by the GCMs (Katzav and Parker, 2015). As a result, outcomes of hydrological climate change impact studies have been reported to become unrealistic without a prior adjustment of climate forcing biases (Ehret et al., 2012; Hansen

et al., 2006; Harding et al., 2014; Sharma et al., 2007). To overcome this limitation, various bias correction techniques have been developed to post-process climate model data to statistically match observations. Bias correction methods are calibrated based on a historical time period for which observations are available. The adjustment is then applied to both the modelled historical period and to the period beyond the time frame of the observations.

Bias correction procedures have mainly focused on adjusting the biases of precipitation and/or temperature (Christensen et al., 2008; Li et al., 2010; Miao et al., 2016; Photiadou et al., 2016; Piani et al., 2010). These variables have traditionally been prioritized for bias correction as they are considered the most important driving variables of hydrological processes in modelling applications – even though from a physical perspective radiation is the driving force of the hydrological cycle. However, many state-of-the-art regional and global hydrological models (GHMs) and land surface models (LSMs) require – apart from precipitation and temperature – additional meteorological forcing, such as solar radiation, air humidity, surface air pressure, and wind speed (a summary of the input variables needed by various hydrological models can be found in the Supplement of Hattermann et al., 2017). For this reason, biases in variables like radiation, humidity, and wind speed can hinder the representation of hydrological fluxes such as runoff, evapotranspiration (ET), snow accumulation, and snowmelt by the impact models (Hagemann et al., 2011; Haddeland et al., 2012), indicating that bias correction should be extended to include more input variables.

Bias correction itself also has limitations, as it is a demanding process in terms of both computational cost and the involved methodological development. Moreover, the use of bias correction is challenged by conceptual pitfalls such as the disruption of the physical consistency of climate variables, the mass–energy balance and the omission of correction feedback mechanisms to other climate variables (Ehret et al., 2012). For these reasons, it is worth examining whether the effect of biases of input variables on hydrological outputs justifies the use of bias correction. Even though this information would be key for making informed decisions on the variables that should be bias corrected for a specific model application, few relevant studies can be found in the literature. Some insight is given by Haddeland et al. (2012), who investigate the combined effect of bias correcting radiation, humidity, and wind speed in addition to precipitation and temperature on hydrological simulations. However, the extent to which individual forcing variable biases affect hydrological simulations and the way that this effect varies spatially are important research questions that remain open.

Here we investigate the effect of the biases in GCM climate variables on the historical runoff output of a large-scale LSM. To this end, we firstly quantify the improvements in the representation of historical modelled runoff when bias corrected variables are used as forcing. Secondly, we exam-

ine the individual effect that the bias of each climate variable can have on runoff simulations. This way we can provide an assessment of the variables beyond precipitation and temperature that may be considered “priority” variables for bias correction, due to their possible pronounced effect on hydrological simulations.

2 Methods

2.1 The JULES land surface model

Hydrological simulations were performed with the Joint UK Land Environment Simulator (JULES) model (Best et al., 2011). JULES is a physically based model that calculates water, energy, and carbon exchanges between the land surface and the atmosphere. The science modules that comprise the model are surface energy fluxes, snow cover and surface hydrology, soil moisture and temperature, soil carbon, vegetation dynamics, and plant physiology. The model requires seven climate variables as forcing, namely, precipitation, temperature, longwave and shortwave radiation, specific humidity, surface pressure, and wind speed. Runoff production in JULES has two components. The first one is surface runoff, produced by the infiltration excess mechanism. The second one is subsurface runoff (or drainage from the bottom of the soil column), which is calculated as a Darcian flux under the assumption of zero gradient of matric potential. Calculation of potential evaporation follows the Penman–Monteith approach (Monteith, 1965). Water held at the plant canopy evaporates at the potential rate, while restrictions of canopy resistance and soil moisture are applied for the simulation of evaporation from soil and plant transpiration from potential evaporation (Best et al., 2011). For a detailed description of JULES, the reader can refer to the model description papers of Best et al. (2011) and Clark et al. (2011). Examples of recent model applications to climate change impact assessments can be found in the studies of Papadimitriou et al. (2016), where JULES is used to investigate future water availability in Europe, and Grillakis et al. (2016), who estimated the climate-induced changes in soil temperature regimes.

2.2 Model set-up and outputs

JULES was run at the global scale, with a spatial resolution of 0.5°. A daily time step was employed for all the model runs. To warm up the model, 10 spin-up cycles from 1973 to 1978 were performed before each main run. The main runs span from 1978 to 2010, but only the time period of 1981 to 2010 is used for the analysis. The model outputs are produced with a daily time resolution.

2.3 Hydrological evaluation

This study focuses on the runoff production output of JULES, hereafter denoted RF. For the assessment of model performance, RF is aggregated at the basin level to allow for comparison with discharge observations. To this end, RF is converted to discharge at the basin outlet (denoted Q) through a delay algorithm proposed by Zulkaffi et al. (2013) and the use of the TRIP river routing scheme (Oki and Sud, 1998) to determine the grid boxes upstream of the basin's outlet.

For the evaluation of JULES' hydrological performance, three metrics are used: Nash–Sutcliffe efficiency (NSE), percent bias (PBIAS), and the coefficient of determination (R^2). The formulas for the calculation of NSE and PBIAS are given in Eqs. (1) and (2):

$$\text{NSE} = 1 - \frac{\sum (Q_{\text{sim}} - Q_{\text{obs}})^2}{\sum (Q_{\text{obs}} - Q_{\text{mean}})^2}, \quad (1)$$

$$\text{PBIAS} = \left[\frac{\sum (Q_{\text{sim}} - Q_{\text{obs}}) \cdot 100}{\sum Q_{\text{obs}}} \right] \%, \quad (2)$$

where Q_{sim} is simulated discharge, Q_{obs} is observed discharge, and Q_{mean} is the mean of observed discharge data. Discharge observations were obtained from the Global Runoff Data Centre (GRDC) database for nine large-scale basins shown in Fig. 1. Information on the basin stations for model evaluation is presented in Table S1 in the Supplement of this paper.

The evaluation metrics are calculated from monthly discharge data. These are the monthly averages of daily discharge for simulations, while observations were obtained in monthly time steps. Model evaluation was based on the historical period from 1981 to 2010. The months missing from the observed discharge time series were neglected from the calculation of the evaluation metrics.

2.4 Climate data

The climate dataset used for bias correction of the GCM data and as a baseline for comparison of the results is the WATCH Forcing Data methodology applied to ERA-Interim data (WFDEI; Weedon et al., 2014). WFDEI data span from 1979 to 2012, but here only the time period from 1981 to 2010 was used. The WFDEI dataset is based on its predecessor WFD (WATCH Forcing Data; Weedon et al., 2010), which was derived from the ERA-40 reanalysis product (Up-pala et al., 2005). For detailed information on the derivation of the WFDEI dataset, the reader is referred to Weedon et al. (2014).

Data from three GCMs participating in the fifth phase of the Coupled Model Intercomparison Project (CMIP5; Taylor et al., 2012) were used as forcing. Information on the ensemble members can be found in Table 1. Climate model outputs were interpolated to the 0.5° spatial resolution of the WFDEI dataset, using the nearest-neighbour method.

2.5 Bias correction method

The bias correction methodology presented by Grillakis et al. (2013), namely multi-segment statistical bias correction (MSBC), is used to adjust the biases in precipitation. MSBC follows the principles of quantile mapping correction techniques and was originally designed and tested for GCM precipitation adjustment. According to the method, the cumulative distribution function (CDF) space is split into discrete segments and then the individual quantile mapping correction is applied to each segment, achieving a better fit of the parametric equations on the data and thus better correction, especially on the CDF edges. The optimal number of segments is estimated by the Schwarz Bayesian information criterion to balance between complexity and performance. A modification of the methodology is used for bias adjustment of the rest of the variables that were used. The modified methodology uses linear functions instead of the gamma functions that were used in the original methodology. This change allows for the facilitation of negative variable values that the gamma functions cannot simulate. Hence, the methodology becomes more universal, to be used in different variable types and distributions. An additional methodological change is performed to the highest and lowest segments' corrections, which are explicitly corrected using only the difference between the historical period model data and the observations. This provides rigidity to the correction, avoiding unrealistic temperature values at the edges of the corrected data CDF. A detailed description and technical details of the modification can be found in Grillakis et al. (2017). As MSBC methodology belongs to the parametric quantile mapping techniques, it shares their advantages and drawbacks. A comprehensive analysis of advantages and disadvantages of the methods that follow the quantile mapping compared to others can be found in Maraun et al. (2010) and Themeßl et al. (2012). The methodology has already been used in in the framework of the ECLISE FP7 (265240) and HELIX FP7 (603864) projects and in a number of climate change impact studies (Grillakis et al., 2016; Papadimitriou et al., 2016). In addition, MSBC has participated in the Bias Correction Intercomparison Project (BCIP) (Nikulin et al., 2015), where it was found to compare well to the other methodologies and was ranked high in performance.

As the bias adjustment involves only the reference period of the GCM data using the same period's observations, its effect is simply limited to the equalization of the cumulative density functions of the raw GCM data towards the WFDEI data. A number of parameter checks were performed on the corrected data, such as prevention of unrealistic values (e.g. negative values to positively constrained variables) and the avoidance of extreme values beyond or below the historical record of WFDEI. The correction was performed separately for each calendar month, keeping physical coherence of the bias adjusted variables, as they are adjusted for their season-

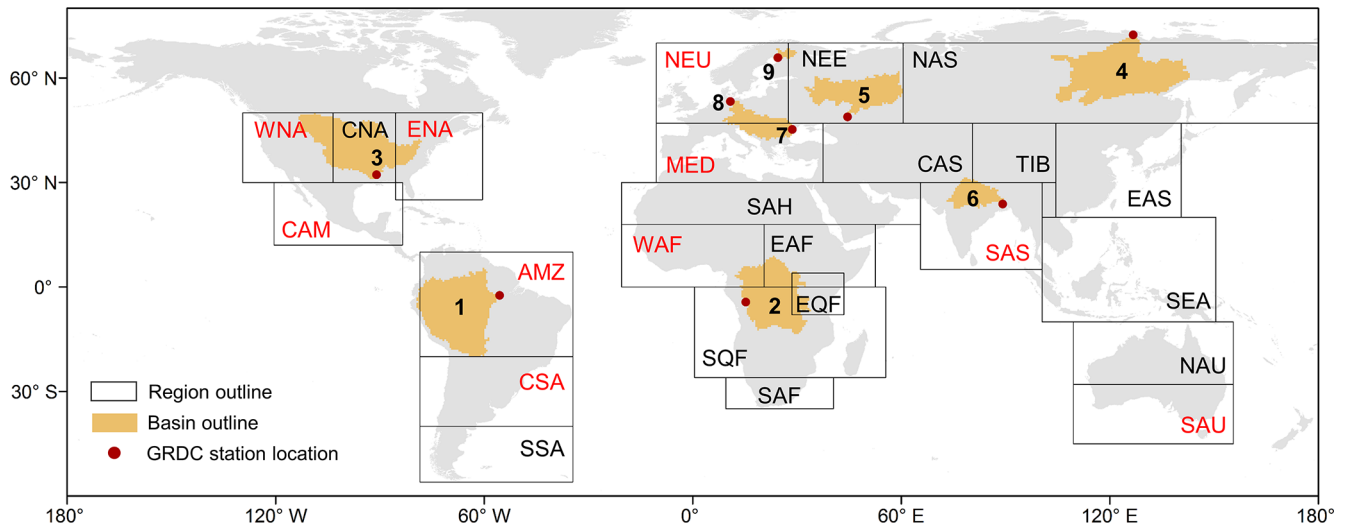


Figure 1. Outlines of study focus regions and hydrological basins and locations of the GRDC gauging stations. With red colour are denoted the regions selected for more detailed analysis. The hydrological basins have been numbered in decreasing order according to their area: (1) Amazon, (2) Congo, (3) Mississippi, (4) Lena, (5) Volga, (6) Ganges, (7) Danube, (8) Elbe, and (9) Kemijoki.

Table 1. Information on the GCMs used for this study.

Modelling group	Institute ID	Model name	$^{\circ}\text{Lon} \times ^{\circ}\text{Lat}$	Key reference
Institut Pierre-Simon Laplace	IPSL	IPSL-CM5A-LR	3.75×1.88	Dufresne et al. (2013)
Japan Agency for Marine-Earth Science and Technology, Atmosphere and Ocean Research Institute (The University of Tokyo), and the National Institute for Environmental Studies	MIROC	MIROC-ESM-CHEM	2.81×2.81	Watanabe et al. (2011)
US Dept. of Commerce/NOAA/Geophysical Fluid Dynamics Laboratory	GFDL-NOAA	GFDL-ESM2M	2.50×2.00	Dunne et al. (2012)

ality in a coherent way according to the observational dataset that is used.

2.6 Experimental design

In order to examine the effect of each forcing variable's bias on runoff we designed and implemented an experiment comprised of two parts (bias assessment and partial correction bias assessment) and nine sets of JULES' runs in total. A graphical description of the performed experiment is shown in Fig. 2. Climate data from three GCMs and the WFDEI dataset are used as JULES' forcing. The sets of runs forced with GCM data include three model runs – one per GCM. Then the analysis progresses using the ensemble mean. The time span of this analysis is the historical period 1981–2010. This is also the time span of the period used for bias correction of the GCM output.

2.7 Bias assessment

The first part of the experiment is to assess initial and remaining biases in the forcing data and in simulated runoff. Initial bias refers to the difference between raw GCM variables and the respective WFDEI variables. Remaining bias is the bias in the forcing variables after the bias correction, i.e. the difference between bias corrected GCM variables and the respective WFDEI variables. Referring to runoff, “initial” and “remaining” biases are defined as the difference between runoff simulations forced with raw and bias corrected forcing respectively from simulations forced with the WFDEI dataset. This definition is employed to shorten and simplify the expressions used in this paper (i.e. “initial bias in runoff” instead of “the difference between runoff forced with raw GCM data and WFDEI data”). In this part of the experiment, three sets of JULES' runs were conducted:

- i. forced with WFDEI (WFDEI);
- ii. forced with uncorrected climate data (raw); and

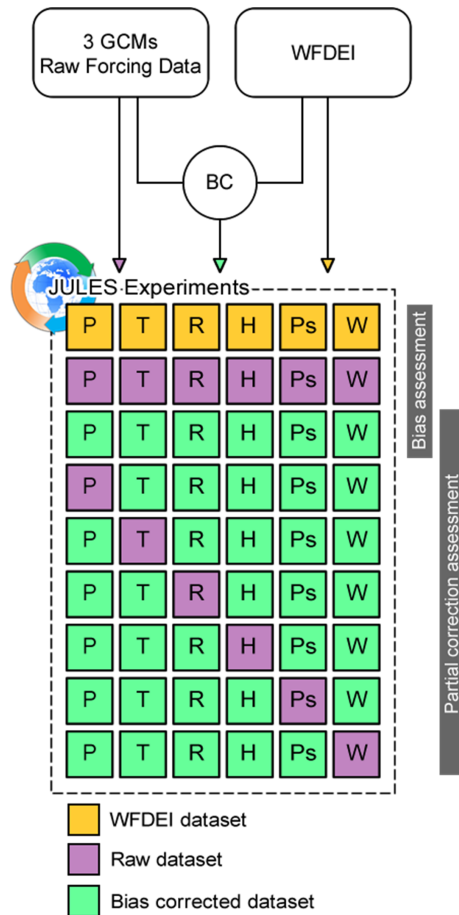


Figure 2. Graphical description of the performed experiment.

iii. forced with bias corrected climate data (BC).

2.8 Partial correction bias assessment

For the second part of the experiment – the partial correction bias assessment – six more sets of JULES’ runs were performed. In each of these runs, one of the six forcing variables (precipitation, temperature, radiation, humidity, surface pressure, and wind speed) is used in its raw form, while the rest of the input forcing is bias corrected. The partial correction assessment runs are symbolized as NobcV (NOt Bias Corrected variable *V*), where *V* is one of the six forcing variables: precipitation (*P*), temperature (*T*), radiation (*R*), specific humidity (*H*), surface pressure (*Ps*), and wind (*W*). It has to be noted here that downward longwave radiation (*Rl*) and downward shortwave (*Rs*) were examined together; hence, in the respective NobcR run, both downward shortwave and downward longwave radiation were forced in uncorrected form. Partial correction assessment is composed as a tool to quantify the individual effect of each forcing variable on runoff, but is not designed to suggest and assess run formats.

The simulated runoff of each partially corrected input is compared to the respective simulation in which all input variables are bias corrected (denoted as BC). This comparison allows us to assess the “loss” of the performance of simulations when a variable is neglected from the bias correction procedure. It must be noted however that the “loss of performance” concept bears the assumption that the BC simulation is closer to the WFDEI simulation compared to a partially corrected set.

2.9 Categorization of individual variable bias effects

A new framework for the classification of the effects of forcing variables’ biases on modelled runoff is developed and implemented. The classification employs the comparison of the bias in each forcing variable (ΔV) and the corresponding relative effect in simulated runoff (ΔRF), discretizing four different categories (Fig. 3). To facilitate the comparison among the different forcing variables, ΔV and ΔRF are expressed as percentages. More specifically, ΔV and ΔRF are defined as follows.

ΔV is the difference between the raw and bias corrected variable value, divided by the bias corrected variable value. ΔV is estimated by Eq. (3).

$$\Delta V = \frac{\text{raw variable} - \text{BC variable}}{\text{BC variable}} \cdot 100\% \quad (3)$$

As an exception, for temperature ΔV refers to the absolute difference between raw and bias corrected temperature (in K).

ΔRF expresses the effect of a variable’s bias on runoff and is calculated from the difference between runoff forced with all bias corrected variables except for the examined variable *V* (NobcV) and runoff forced with all bias corrected variables (BC), divided by the runoff of all bias corrected variables (BC). ΔRF is estimated by Eq. (4).

$$\Delta RF = \frac{\text{RF from NobcV} - \text{RF from BC}}{\text{RF from BC}} \cdot 100\% \quad (4)$$

Sensitivity of runoff to changes in forcing variables (*S*) is the fraction of runoff change over the forcing variable change and serves as a measure to assess the relative magnitude of ΔRF compared to ΔV . When ΔRF is sensitive to ΔV , relatively smaller changes in the variable should cause relatively larger changes in runoff and vice versa. Sensitivity is in general dimensionless, but for temperature has units of K^{-1} . *S* is estimated by

$$S = \Delta RF / \Delta V. \quad (5)$$

In total, there are six sets of ΔV s and six sets of ΔRF s, one for each examined variable and experiment respectively, and six sets of sensitivities (*S*). The absolute values of ΔV , ΔRF , and *S* denoted $|\Delta V|$, $|\Delta RF|$, and $|S|$ are used to avoid dealing with the sign of the changes and rather focus on their magnitude.

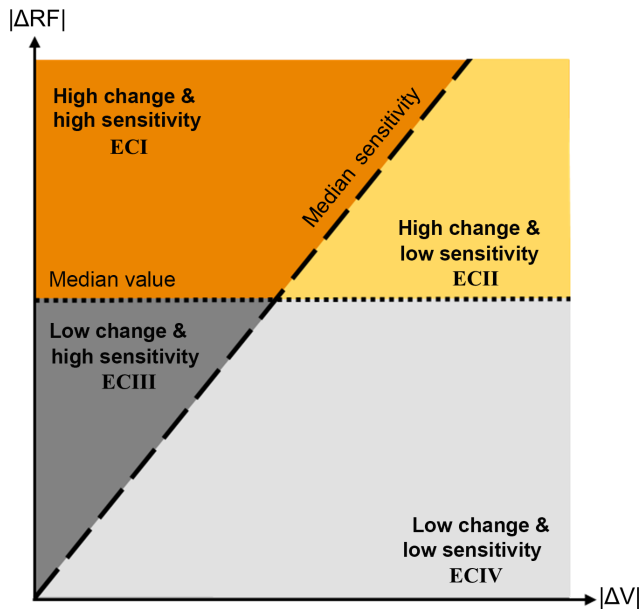


Figure 3. Categorization of the effect of changes in forcing variables (V) on runoff (RF). The four areas correspond to the four defined effect categories. The x axis corresponds to relative changes in forcing variables and the y axis to relative changes in runoff. For all changes, the absolute value is considered.

As shown in Fig. 3, the effect of each variable's bias ($|\Delta V|$) on runoff ($|\Delta RF|$) is separated into four different categories according to two rules. The first rule is the characterization of $|\Delta RF|$ among all the experiments as “low” or “high” relative to its median value, shaping the ordinate $y = \text{median}(|\Delta RF|)$. $\text{Median}(|\Delta RF|)$ is derived considering the $|\Delta RF|$ values of all land grid boxes and for all the experiments. The second rule is the characterization of sensitivity $|S|$ as high or low relative to its median value. The latter forms a bisectrix $s = \text{median}(|S|)$. $\text{Median}(|S|)$ is, accordingly to $\text{median}(|\Delta RF|)$, derived from the $|S|$ values of all grid boxes and for all the experiments apart from temperature. In the case of temperature, $\text{median}(|S|)$ is explicitly recalculated from the values of all the land grid boxes of this specific experiment. These two rules form the four categories of Fig. 3. Combinations of the two rules result in four different effect categories (ECs) presented in decreasing order of the effect of a variable's bias on runoff:

- i. High change and high sensitivity (ECI);
- ii. high change and low sensitivity (ECII);
- iii. low change and high sensitivity (ECIII); and
- iv. low change and low sensitivity (ECIV).

2.10 Regional-scale bias assessment

Regional focus is given in 24 regions and 9 hydrological basins. The regions were selected from the 26 regions pre-

Table 2. 24 regions of the globe, selected from Giorgi and Bi (2005).

Region name	Abbreviation
North Europe	NEU
Mediterranean Basin	MED
Northeast Europe	NEE
North Asia	NAS
Central Asia	CAS
Tibet	TIB
Eastern Asia	EAS
Southeast Asia	SEA
Northern Australia	NAU
Southern Australia	SAU
Sahara	SAH
Western Africa	WAF
Eastern Africa	EAF
East Equatorial Africa	EQF
South Equatorial Africa	SQF
Southern Africa	SAF
Western North America	WNA
Central North America	CNA
Eastern North America	ENA
Central America	CAM
Amazon	AMZ
Central South America	CSA
Southern South America	SSA
South Asia	SAS

sented in Giorgi and Bi (2005) (in our study Alaska and Greenland are excluded from the analysis). The hydrological basins were selected to cover different hydro-climatic regimes, in conjunction with GRDC data availability. The selected regions and basins are shown in Fig. 1. The abbreviations of the regions' names can be found in Table 2.

3 Results and discussion

3.1 Long-term annual biases in forcing variables at the global scale

Global maps of the initial and remaining annual biases of the forcing variables are shown in Fig. 4. Respective information on the seasonal biases is presented in Figs. S1 and S2 of the Supplement of this paper. In general terms the remaining annual biases are smaller than the initial ones by 1 to 2 orders of magnitude. For precipitation (Fig. 4a), the largest initial wet biases are observed for regions with high mountain ranges (the Andes in South America, the Alaska Range and the Rocky Mountains in North America, and the Himalayas in Asia) and for the tropical African and Indonesian regions. Only a very small percentage (0.75 %) of the land surface has small biases (-0.01 to 0.01 mm day^{-1}), while the largest biases (> 5 or $< -5 \text{ mm day}^{-1}$) occupy 31.18 % of the land surface. The remaining biases in precipitation are small (up

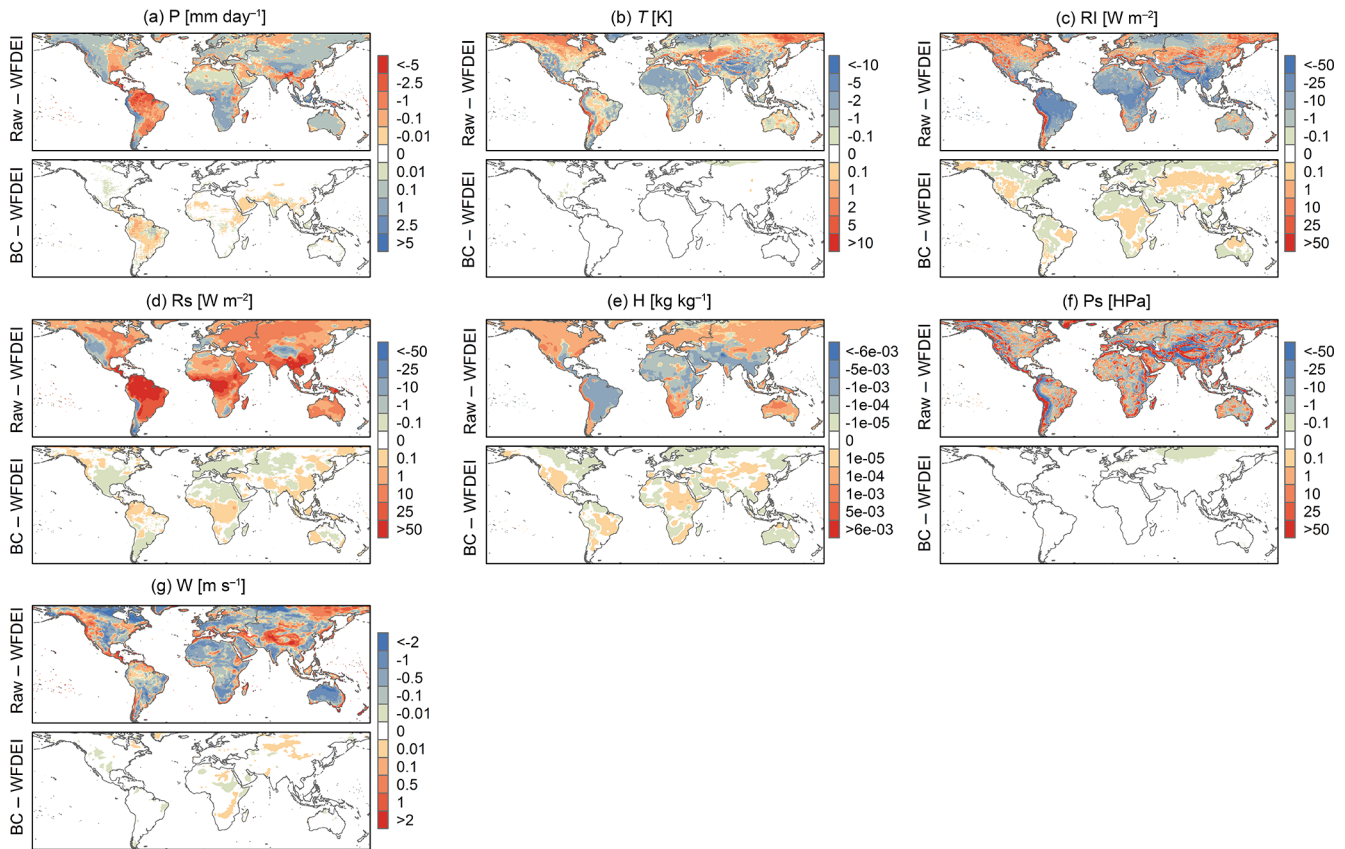


Figure 4. Difference maps, showing initial (raw-WFDEI) and remaining (BC-WFDEI) biases of the GCM ensemble forcing variables: (a) precipitation, (b) temperature, (c) longwave downward radiation, (d) shortwave downward radiation, (e) specific humidity, (h) surface pressure, and (g) wind. Differences are calculated between the long-term annual averages (ANN) of the 1981–2010 period.

to 0.01 mm day^{-1} in absolute terms, for 80.32 % of the land surface) and located in the tropics. The initial biases in temperature are cold biases for 57.82 % of the land surface, while warm biases (mainly found in the Alaskan, Greenland, and northern and central Asia regions, as well as in the Mediterranean and the Andes) occupy 42.12 % of the land surface (Fig. 4b). Initial biases greater than 2 K in absolute terms cover approximately one-third of the land surface (34.74 %). After bias adjustment, the remaining temperature bias is less than 0.1 K for the vast majority of the land surface (97.27 %).

The initial biases of longwave and shortwave radiation (Fig. 4c and d respectively) exhibit similar spatial variations but have different signs. Shortwave radiation shows a greater extent of large biases ($> 50 \text{ W m}^{-2}$ in absolute terms) compared to longwave radiation (8.16 % as opposed to 2.95 % of the land surface). Initial biases in specific humidity are greater than $10^{-3} \text{ kg kg}^{-1}$ (1 g kg^{-1}), in absolute terms, for one-quarter of the land surface (23.65 %) (Fig. 4e). The largest biases in surface pressure (> 50 or $< -50 \text{ hPa}$) occupy 10.01 % of the land surface and are found in the areas where high mountain ranges are located (Rocky Mountains, Andes, Himalayas) (Fig. 4f). The remaining bias in surface pressure is less than 0.1 hPa (in absolute terms) for most of the land

surface (96.50 %). For more than half of the land surface (55.79 %), the wind's initial biases are larger than 0.5 m s^{-1} or smaller than -0.5 m s^{-1} (Fig. 4g). The remaining biases of the wind variable range between -0.01 and 0.01 m s^{-1} for the majority of the land surface (87.71 %).

Generally, the initial GCM biases in precipitation and temperature are more pronounced over high mountainous regions and the tropics. Recent studies argue for a dependency between biases and altitude. According to the study of Haslinger et al. (2013), temperature and precipitation biases of a GCM tested over the Alpine region both show increasing trends with height. Regarding the tropics, various studies show increased GCM biases in these regions compared to model performance in other climate zones (Koutroulis et al., 2016; Randall et al., 2007; Solman et al., 2013). The initial surface pressure biases are also linked to altitude, as surface pressure heavily depends on elevation. Initial biases in surface pressure have a similar elevation pattern and could be a result of the different spatial resolutions of the elevation model in the GCMs and WFDEI. The WFDEI dataset resolution is 0.5° , while the original GCM spatial resolution is considerably lower (around 2.5°). GCM surface pressure is simulated taking into account a relatively low-resolution

elevation model. Although GCM surface pressure is interpolated to the WFDEI resolution, this does not correct the elevation-induced error in the GCM simulations.

The remaining biases in precipitation in the tropical regions were also identified and discussed extensively by Grilakis et al. (2013) and are related to the error in the CDF approximation during bias correction. For the rest of the variables, the remaining bias, although not actually zero, is very close to zero (well below the smallest positive and above the smallest negative rank in the legend, e.g. below -0.1 K and below 0.1 K for temperature). The colour scale in Fig. 4 was selected with the intention of showing the remaining biases, but this does not mean that their values are accountable. They are rather trace errors occurring due to truncation numerical errors during the bias correction process. Hence the remaining biases (except for precipitation) could not be attributed to a specific mechanism.

3.2 Regional and seasonal biases in forcing variables

Figure 5 illustrates the initial biases of the GCM ensemble, spatially aggregated over 24 regions of the globe. To account for possible seasonality variations, the biases are calculated for the annual mean (ANN) and for the December–January–February (DJF) and June–July–August (JJA) means. The remaining biases are not shown because their regionally aggregated values are negligible and would be indistinguishable in the figure. Additionally, an insight into the behaviour of each ensemble member, in comparison to the ensemble mean and WFDEI, is given by Table S2. Table S2 provides the values of raw input variables for each ensemble member, the ensemble mean value, and the respective WFDEI value, averaged for the 24 study regions.

Precipitation biases are less pronounced in Europe (NEU, MED, and NEE) and in central and northern Asian regions (CAS and NAS). The wettest precipitation biases are encountered in equatorial and southern Africa (EQF, SQF, and SAF) and concern DJF precipitation (Fig. 5). The driest biases are found for the CAM, AMZ, and SAS regions, for JJA precipitation. Temperature displays cold biases in most regions. A notable exception is the warm bias in DJF temperature in the NAS region, which is the most pronounced temperature bias found. Generally the DJF temperature biases are the largest, followed by ANN, while the JJA season has the smallest temperature biases.

The two radiation components, longwave (RI) and shortwave (Rs) radiation, show an inverse behaviour in their biases (Fig. 5). That is to say, in regions where RI has negative biases, Rs exhibits positive biases and vice versa. According to Demory et al. (2014), overestimation of shortwave radiation is a common issue amongst the GCMs. Negative biases are dominant for RI, in contrast to the Rs variable, which mostly shows positive biases. Specific humidity has negative biases over the northern part of the African continent (SAH, WAF, EAF, and EQF), Central and South America (CAM,

AMZ, and CSA), and South Asia (SAS). Positive humidity biases are identified in the southern part of Africa (SQF and SAF) and North America (WNA, CNA, and ENA).

Surface pressure shows almost exclusively positive biases (Fig. 5). The regions that distinguish for the largest biases are MED, SEA, SAH, SAF, CAM, CSA, and SSA. The most dominant negative wind speed bias is found in NAU. Most of the African continent (SAH, WAF, EAF, EQF, and SQF) and of South America (AMZ and CSA) also have negative biases in wind. The largest positive biases are encountered in the southern part of South America (SSA) for the JJA season and for the DJF season in regions of North America (WNA and CAM), Europe (MED), and Asia (CAS, TIB, and SEA).

3.3 Model evaluation

In order to assess JULES' performance, we compare discharge modelled with WFDEI and with the raw GCM dataset to discharge observations for nine study basins. Figure 6 shows the seasonality of observed and modelled discharge and the evaluation metrics of the two sets of simulations (WFDEI and raw GCM) are presented in Table 3.

For seven out of the nine basins (Amazon, Congo, Volga, Ganges, Danube, Elbe, and Kemijoki) seasonality is captured well by the WFDEI simulation (Fig. 6). In contrast, the raw GCM simulation exhibits significant positive and negative biases for these seven basins. For the two remaining basins, however (Mississippi and Lena), seasonality is better captured by the raw GCM simulation. The WFDEI run results in positive NSE values (0.24 to 0.94) for all the basins. By contrast, the raw GCM run results in negative NSE values for six out of the nine basins. PBIAS indicates that the raw GCM simulation exhibits greater deviations from observations than the WFDEI run for most basins (exceptions are the Mississippi, Lena, Ganges, and Danube). Finally, the R^2 metric shows that the linear correlation between simulations and observations is stronger for the WFDEI run for seven out of the nine basins (exceptions are the Mississippi and Elbe). For both simulations the lowest R^2 value is reported for the Congo basin (0.45 and 0.2 for the WFDEI and raw GCM runs respectively). The best correlations per simulation are found for the Ganges for the WFDEI run (0.99) and for the Amazon for the raw GCM run (0.94).

The shown persistent departure from the mean climatology of discharge could include three types of errors. The first is the error stemming from the insufficient description of the runoff processes by the land surface model and from the routing algorithm (Blyth et al., 2011). The second type of error is a result of errors in the forcing datasets (either observational or GCM output) with regards to depicting the real climatic drivers (Elsner et al., 2014; Mizukami et al., 2014). A third possible error comes from the comparison of naturalized discharge of the simulations with measured discharge due to influences like abstractions and dams regulating the natural river flow (Müller Schmied et al., 2014). An extra

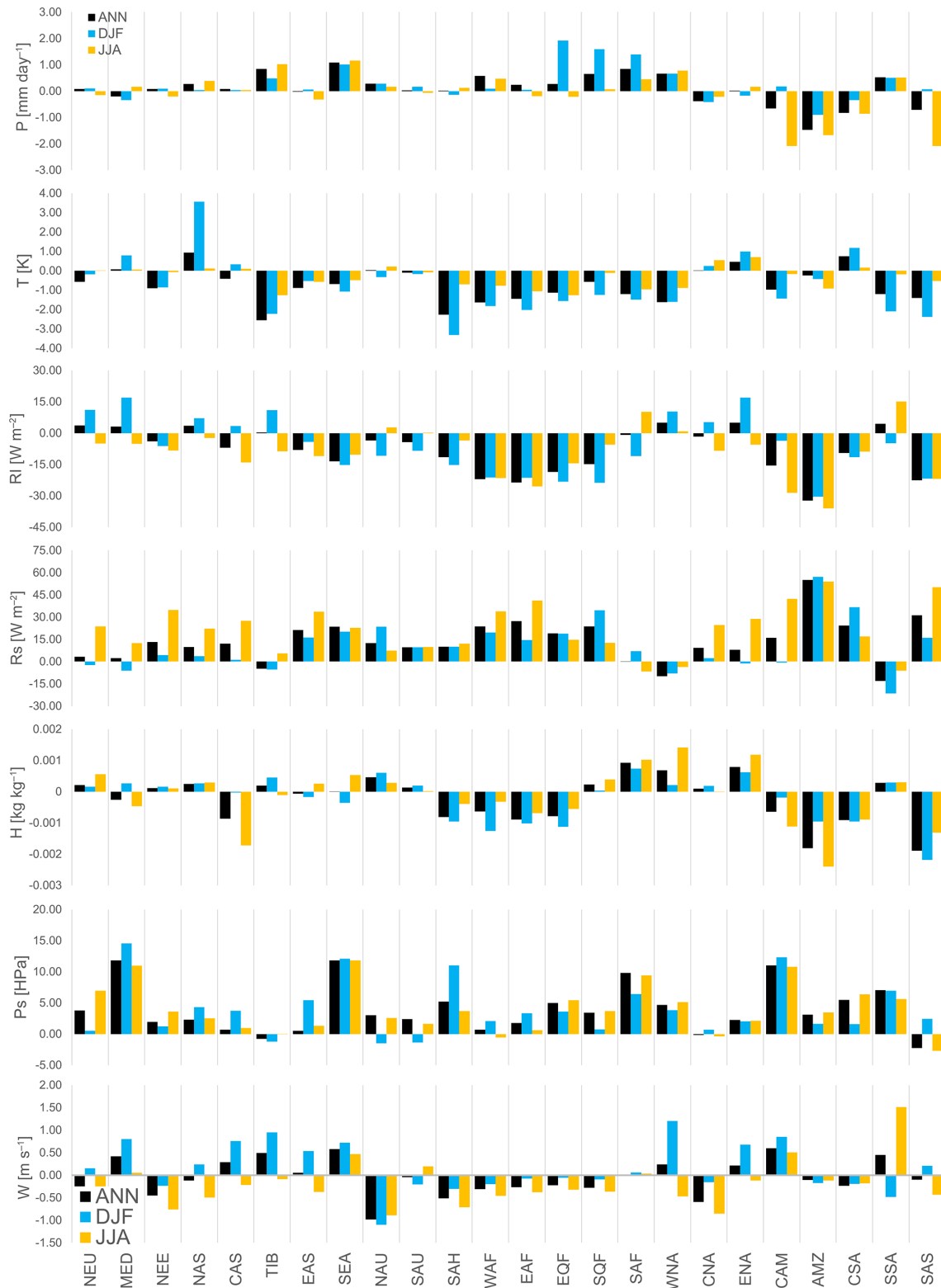


Figure 5. Initial biases (raw-WFDEI) of the GCM ensemble forcing variables, spatially averaged for 24 Giorgi regions. Biases are calculated between long-term annual averages (ANN) and December–January–February (DJF) and June–July–August (JJA) averages of the period 1981–2010.

Table 3. Evaluation metrics derived from monthly discharge data. Metrics are calculated for JULES' simulations from WFDEI data (WFDEI) and the ensemble mean of raw GCM data (raw EM).

Indices	NSE		PBIAS		R^2	
	WFDEI	Raw EM	WFDEI	Raw EM	WFDEI	Raw EM
Amazon	0.48	−2.66	−18.68	−51.84	0.96	0.94
Congo	0.39	−36.40	4.06	116.77	0.45	0.20
Mississippi	0.24	0.90	21.56	−4.46	0.73	0.92
Lena	0.56	0.82	−39.32	32.14	0.98	0.89
Volga	0.82	−1.42	−17.09	35.12	0.95	0.66
Ganges	0.94	0.80	19.48	−9.51	0.99	0.91
Danube	0.28	−1.51	15.20	1.14	0.88	0.19
Elbe	0.67	−26.04	8.28	179.83	0.81	0.86
Kemijoki	0.91	−0.98	8.55	66.50	0.94	0.89

error component, which is not considered here, could result from the uncertainty in discharge measurements (Coxon et al., 2015).

The model evaluation has revealed two basins (Mississippi and Lena) for which raw GCM forced discharge simulations outperform the WFDEI simulations. For the Mississippi, the WFDEI run gives higher discharge than the observations throughout the year, revealing a deficiency of the model in capturing the water balance of this basin. Most of the Mississippi extent is in the CNA region, where negative precipitation biases have been documented (Fig. 5). Thus, the raw GCM run is forced with less precipitation compared to WFDEI and less discharge is produced, masking the model deficiency in this basin and improving the metrics of model performance. It is also important to note that the range of the raw GCM simulations is quite broad, especially for a three-member ensemble. The upper range of the GCM ensemble exceeds the WFDEI-simulated runoff during almost half the seasonal cycle. This indicates that the individual ensemble members would not necessarily outperform the WFDEI run and that, for this specific basin, the ensemble averaging has possibly produced a “false positive” in model performance. In this particular basin, model performance may also be hindered due to the comparison of naturalized and actual discharge, as the Mississippi is a heavily regulated river. For the Lena, the WFDEI run underestimates measured discharge by about 40%. The Lena basin falls into the extent of the NAS region, for which positive precipitation biases have been documented (Fig. 5). The extra water in the raw GCM run counteracts the tendency of the model to underestimate discharge in the Lena basin, resulting in an improved model performance. In the context of the present study we are not able to identify the exact reasons why model performance is hindered in some basins. It is unrealistic for a global LSM to achieve top performance around the world (Hattermann et al., 2017), as, due to its global nature, some fixes in some regions could result in deteriorations in performance in other parts of the land surface. Thus, the interpretation of the following

analysis of the present study should consider the model deficiencies revealed in this section.

3.4 Long-term biases in runoff at the global scale

Figure 7 shows the initial and remaining biases in runoff, derived from ANN, DJF, and JJA long-term means. As with the biases in the input forcing variables, the remaining bias in runoff is 1 to 2 orders of magnitude smaller than the initial bias. Hence, the use of bias corrected data led to an improved representation of runoff by the model, compared to the baseline of the WFDEI run. Accordingly, the studies of Teutschbein and Seibert (2012) and Rojas et al. (2011) found that hydrological simulations are substantially improved with the use of bias corrected forcing.

Regarding the raw GCM run, the largest runoff underestimation biases ($< -5 \text{ mm day}^{-1}$) are encountered in Central and North America, the central–eastern part of South America, and East Asia. The most pronounced runoff overestimation biases are found in the western part of North and South America, in equatorial and southern Africa, northern Europe, the Tibetan region, and Indonesia. Initial runoff biases are larger than 1 mm day^{-1} in absolute terms for 16.26, 14.85, and 20.18% of the land surface respectively for ANN, DJF, and JJA. The differences between the seasonal means (DJF, JJA) and the annual mean (ANN) are in general subtle. However, the increases in runoff overestimation biases in DJF in southern equatorial Africa and in JJA in the Tibetan plateau are worth noting. Large initial biases ($> 5 \text{ mm day}^{-1}$ in absolute terms) in seasonal means occupy a greater percentage of the land surface compared to the annual mean (0.70% for ANN, compared to 1.25 and 1.97% for DJF and JJA respectively).

The remaining biases in runoff range from -0.1 to 0.1 mm day^{-1} for the majority of the land surface (95.19, 87.40, and 80.30% for ANN, DJF, and JJA respectively). Negligible biases (smaller than 0.01 mm day^{-1} in absolute terms) are found for more than one-third of the land surface (specifically for 38.06% of the land area for ANN, 37.60%

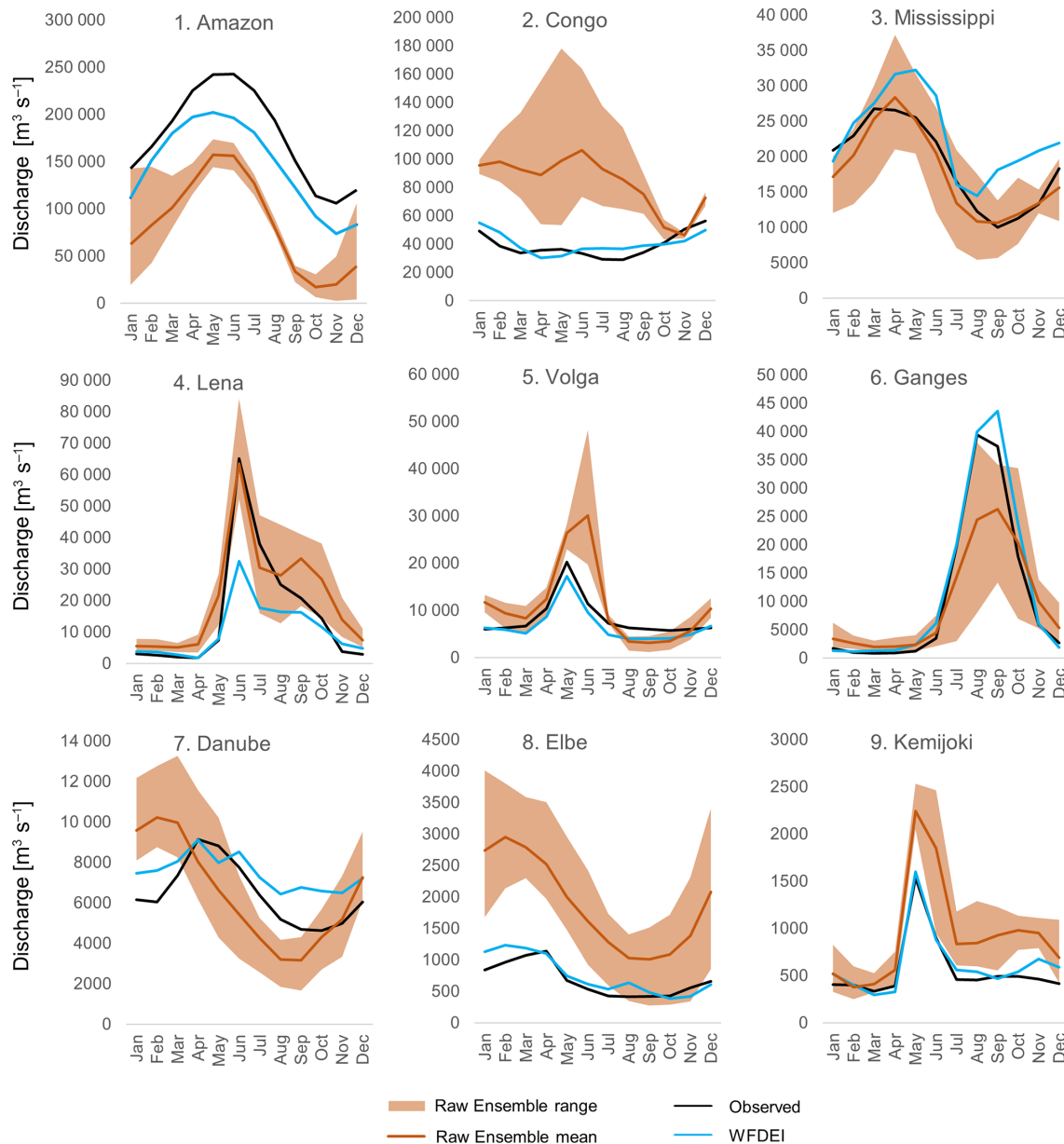


Figure 6. Discharge seasonality ($\text{m}^3 \text{s}^{-1}$) derived from the period 1981–2010 for nine study basins. Each panel shows observed discharge (GRDC measurements) compared to JULES’ simulated discharge from WFDEI data and raw GCM data (the mean and the range of the ensemble are shown).

for DJF, and 34.42 % for JJA). The (negative) remaining bias in ANN runoff is more pronounced in the western Amazonian region. This probably corresponds to the remaining bias in precipitation identified for the Amazonian region (Fig. 4). In addition to the significant reduction of the biases in runoff forced with bias corrected data, it can be observed that the remaining biases have switched signs compared to the initial biases. This means that in regions where the initial bias in runoff is positive (negative), the raw GCM forced runoff is larger (smaller) than runoff forced with WFDEI, and the use of bias corrected forcing results in runoff slightly lower

(higher) than WFDEI runoff. A respective behaviour was not observed in the initial and remaining biases of the most impacting forcing variables (P and T), but it was, to an extent, present for other variables (RI , Rs , and H). Thus, the “over-correction” manifested for bias corrected runoff compared to WFDEI runoff cannot be attributed to remaining biases in precipitation and temperature. Instead, it could plausibly be associated with the compound effect of the remaining biases in some (or in all other) forcing variables.

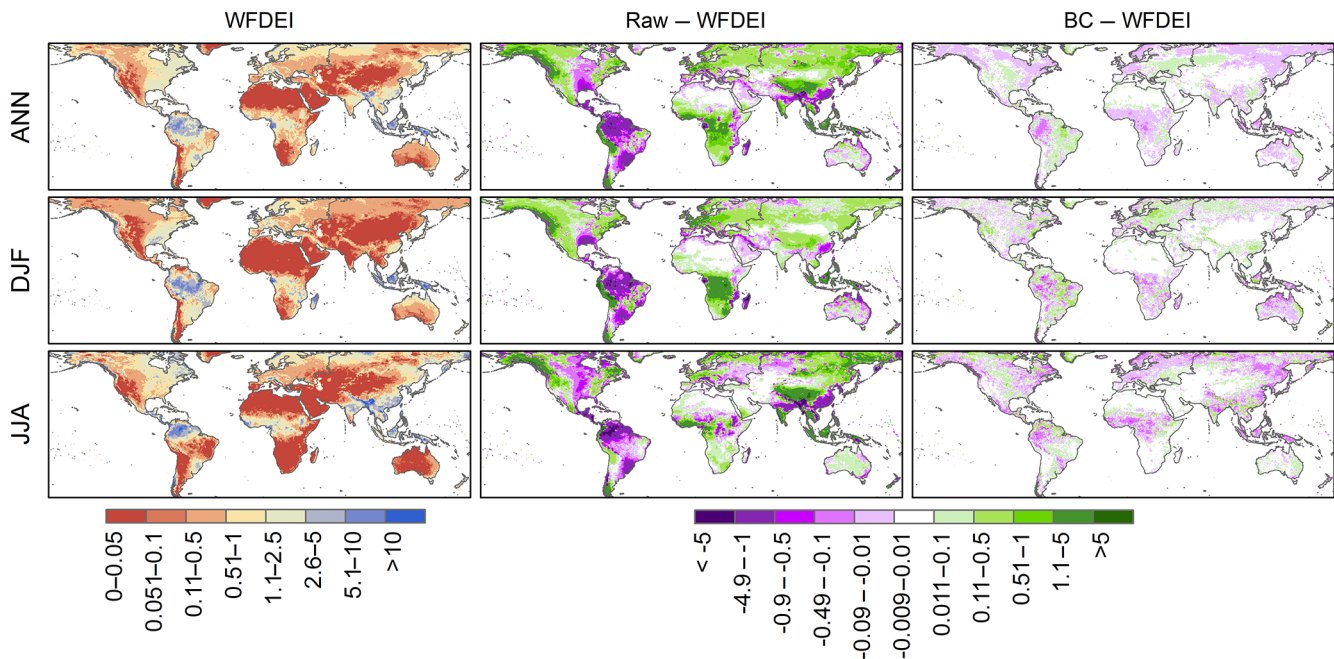


Figure 7. Runoff (mm day^{-1}) from WFDEI data (left column). Initial (raw-WFDEI) and remaining (BC-WFDEI) biases in runoff are shown in the middle and right columns respectively. Results are shown for long-term annual averages (ANN) and for December–January–February (DJF) and June–July–August (JJA) averages of the 1981–2010 period.

3.5 Effect of each forcing variable's bias on runoff

The effect that the bias of each forcing variable can have on runoff is investigated here, by comparing runoff from the bias corrected run to the partial correction assessment runs. The results are shown in Fig. 8, for ANN, DJF, and JJA averages.

First, we discuss the runoff differences calculated from the ANN period. Precipitation and temperature are the only two variables that cause runoff differences larger than 5 mm day^{-1} (in absolute terms) when neglected from bias correction. However, these differences regard a very small percentage of the land surface: 0.61 % for precipitation and only 0.02 % for temperature. Moreover, precipitation bias causes changes in runoff greater than 1 mm day^{-1} (in absolute terms) for 14.28 % of the land area. Such changes for the other variables occupy a significantly smaller fraction of the land area (ranging from 1.21 % for temperature to 0.05 % for wind). Based on the above it can be stated that precipitation is the variable that most affects runoff response. Precipitation bias causes both wet and dry biases in different regions of the land surface, with a pattern that closely resembles the effect of the initial GCMs' biases on runoff (Fig. 7). A similar pattern between precipitation and runoff biases was also observed by Teng et al. (2015), who noted that precipitation errors are magnified in modelled runoff. Temperature biases result in runoff overestimation for around 60 % of the land surface (e.g. over western and eastern North America, the Amazon region, equatorial Africa, northern Europe, and parts of Asia) and runoff underestimation for around 40 % (example

regions: parts of Central and South America and of central Asia). Temperature biases correspond to small changes in runoff (up to 0.01 mm day^{-1} in absolute terms) over about one-third of the land area. Excluding the radiation components from the bias correction procedure produces negative runoff changes for the majority of the land surface (67.60 %), while for around 80 % of the land surface the differences in runoff range between -0.1 and 0.1 mm day^{-1} . The bias in the specific humidity variable corresponds to runoff overestimations for 64 % of the land area. The areas of runoff overestimation are mainly located at the higher latitudes (northern part of North America, Europe, and northern Asia). For 36.43 % of the land surface, changes in runoff due to specific humidity biases span between 0.1 and 0.5 in absolute terms. Surface pressure and wind are the variables that show the smaller effect on the hydrological output, as their exclusion from bias correction corresponds to small changes in runoff (less than 0.1 mm day^{-1} in absolute terms) for the vast majority of the land surface (around 94 and 92 % of the land surface respectively for surface pressure, and wind speed). The most pronounced differences in runoff due to surface pressure biases are negative and are encountered over the high mountain range regions of South America and Asia (Andes and Himalayas respectively).

The patterns of runoff changes due to the biases of the forcing variables derived from annual (ANN) and seasonal (DJF, JJA) averages show only subtle variations. In general the above analysis of the ANN runoff differences applies also

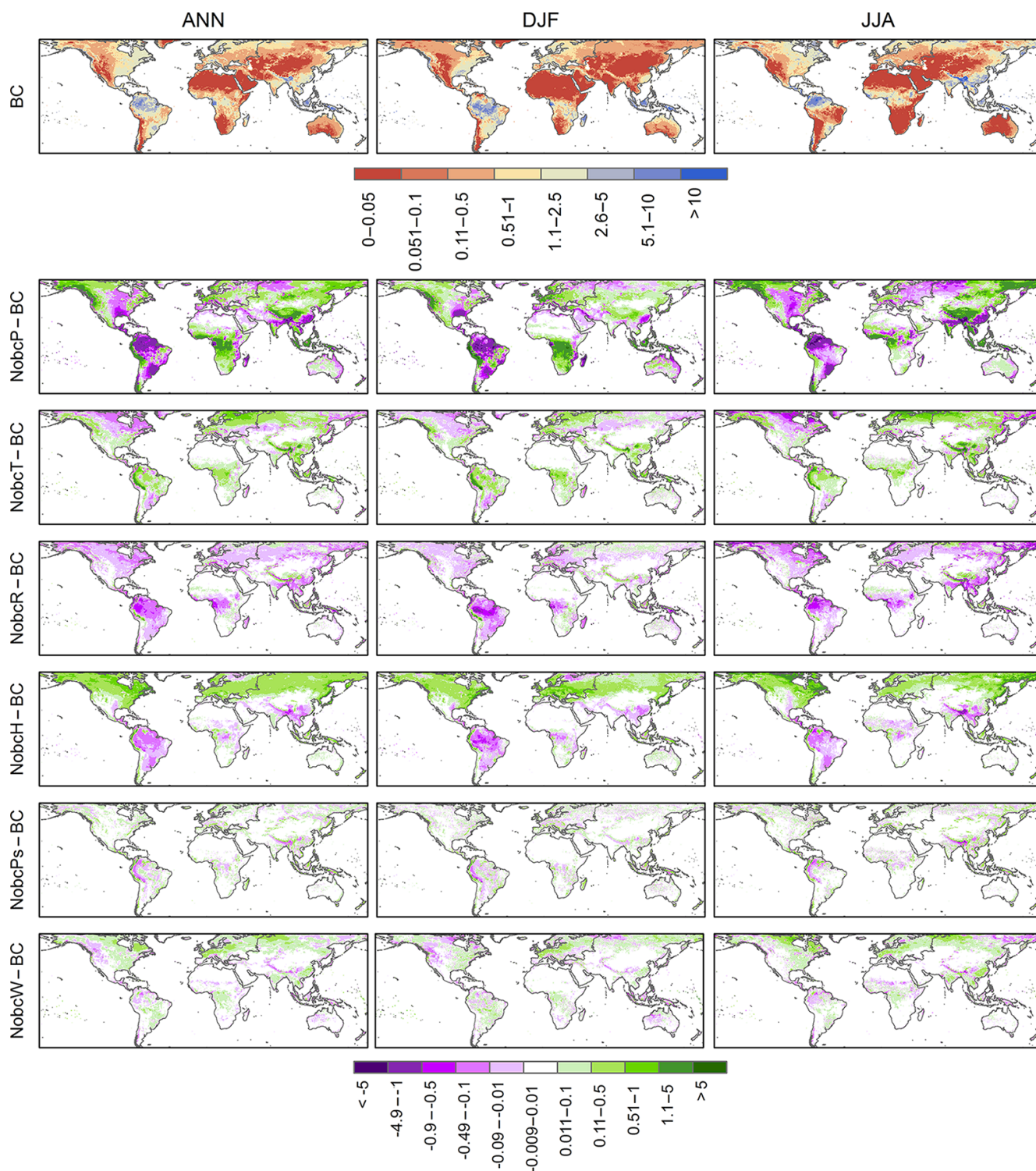


Figure 8. (Top row) Runoff (mm day^{-1}) from bias corrected GCM ensemble forcing (BC) and (second to last row) runoff differences between the bias corrected run (BC) and the partially corrected runs (NobcV, where V is one of the forcing variables P, T, R, H, Ps, or W). Results are shown for long-term annual averages (ANN) and for December–January–February (DJF) and June–July–August (JJA) averages of the 1981–2010 period.

to the seasonal values, with small variations on the land fractions that show a specific response to forcing biases.

From this analysis it can be deduced that apart from the main hydrological cycle drivers (precipitation and temperature), radiation and specific humidity can also have a substantial effect on runoff, especially for specific regions. These findings will be further investigated and discussed in the following sections. Other studies also advocate the considerable effect that biases in radiation (Mizukami et al., 2014) and humidity (Masaki et al., 2015) can have on hydrological fluxes.

3.6 Runoff sensitivities to forcing variables

Sensitivity of runoff changes to the biases of the forcing variables is examined by exploring the relationship between the input forcing biases (ΔV) and the corresponding changes in runoff (ΔRF). The regional variation of this relationship is also investigated. Figure 9 shows scatterplots of ΔRF versus ΔV for each examined variable, for 10 selected regions. The dots in each scatterplot correspond to the land grid boxes of each region. The presented regions are selected as representative of different parts of the land surface, as the number of the regions shown in the manuscript had to be reduced for clarity of the results. Scatterplots of the 24 examined regions can be found in the Supplement of this paper (Fig. S3). The median values of ΔV , ΔRF , and S of the land grid boxes of each region, for the 24 examined regions, are shown in Table 4.

The correlation between the six ΔV s and respective ΔRF s differs substantially between the examined regions. Generally, the correlations show a non-uniform behaviour, identified by the highly scattered data clouds. This implies a high spatial variability of runoff sensitivity to the examined variables.

For precipitation, the ΔRF over ΔP relationship exhibits a non-linear behaviour, indicating that the relative change in runoff is not proportional to precipitation bias, but also depends on the magnitude of precipitation bias. Renner et al. (2012) also identified non-linearities in the relationship between relative changes in streamflow and changes in precipitation, and argued that non-linear behaviour is a result of the combined effects of water and energy balances. Temperature biases have an inversely proportional and highly non-linear relationship with changes in runoff. The ΔRF over ΔT relationship is also variant for different regions. For example, the scatterplots for NEU and WNA indicate that small temperature biases may correspond to large changes in runoff. In contrast, the scatterplot for CAM indicates that larger temperature biases correspond to smaller changes in runoff compared to the other regions. Radiation biases are small but can correspond to high changes in runoff for some regions (WNA, SAS, WAF, and AMZ). For specific humidity it can be observed that small positive biases correspond to high changes in runoff for some regions (NEU, MED, WNA, and ENA). A different behaviour is observed for CAM, SAS,

AMZ, and CSA, where the data cloud is more scattered on the x axis (meaning larger biases in specific humidity) and less scattered on the y axis (i.e. changes in runoff are smaller). Surface pressure has smaller biases compared to the other forcing variables and its effect on runoff also appears reduced. Wind has a wide range of both positive and negative biases which, however, do not seem to affect runoff accordingly.

The variation of the ΔRF over ΔV relationships across the different regions can be attributed to a number of factors. First, it depends on the magnitude and signal of the biases in the forcing variables. As previously shown, these can have significant spatial variations (Fig. 4). For example, according to the median values of relative changes in Table 3, some regions are dominated by negative precipitation biases (MED, SAS, AMZ, and CSA) and others by positive biases (NEU, WNA, ENA, CAM, WAF, and SAU). Second, it reflects the climatology of each region. The same biases would affect differently regions with different runoff (and evapotranspiration) fractions of each region. The precipitation partitioning to runoff and evapotranspiration is a climate characteristic and is controlled by either water or energy limitations, depending on the region. Additionally, we should consider that although we assess the effect of long-term annual biases on long-term annual runoff, the results are still dependent on the seasonal cycles of the variables and/or runoff, especially if the seasonality of precipitation in the region is strong. For example, the same annual bias in temperature would translate differently to runoff changes in a region with precipitation evenly dispersed throughout the year and in another region where most of the annual precipitation happens during the summer months. Finally, as this is a model-based experiment, we should consider whether high sensitivities of some variables for specific regions are a result of over-sensitivity of the model. Vano et al. (2012) documented considerable differences in the spatial distribution of sensitivities to precipitation modelled by five LSMs.

3.7 Spatial distribution of bias effect categories

Figure 10 shows global maps of bias ECs for each forcing variable, derived according to the methodology described in Sect. 2.8. The land area fraction corresponding to each EC is tabulated in Table 5.

Precipitation is the variable whose biases have the largest effect on runoff, with the vast majority of the land surface (92 %) corresponding to the high change categories ECI (67.80 %) and ECII (24.20 %). Radiation has the second largest land fraction in ECI, but temperature has the second largest land fraction in the high change categories (ECI and ECII). Radiation also has the largest land fraction in the high sensitivity categories (ECI and ECIII). As discussed in Sect. 3.6, this is possibly a result of combining shortwave and longwave radiation for the calculation of the radiation biases. For specific humidity, the most affected areas (ECI)

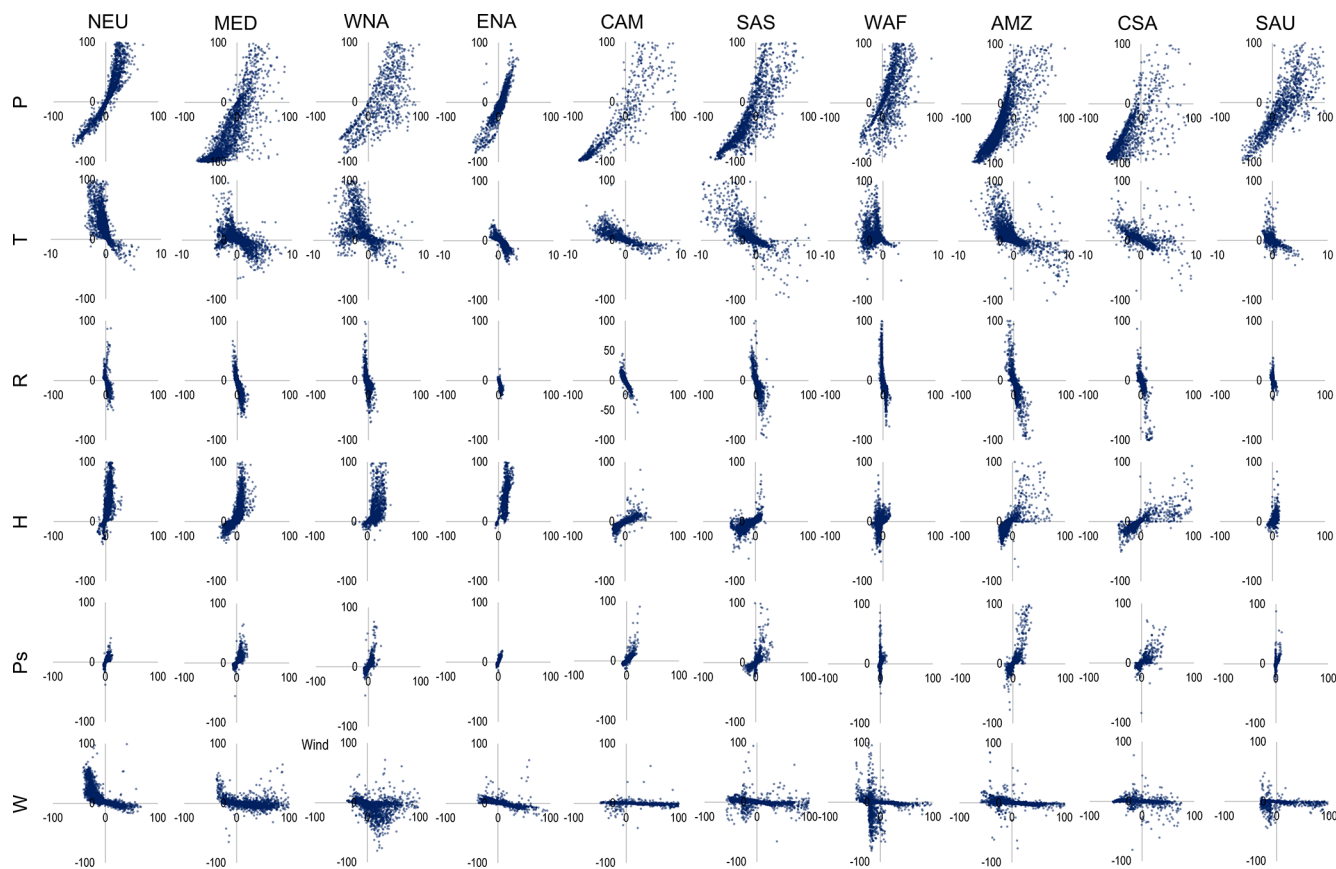


Figure 9. Scatterplots of relative changes in the forcing variable (ΔV , x axis) and corresponding relative changes in runoff (ΔRF , y axis), for all the forcing variables and for selected regions. In each panel, each dot represents the $\Delta RF / \Delta V$ relationship of each land grid box in the examined region.

show a significant spatial coherence and are clustered at the higher latitudes of the globe. Surface pressure biases belong to ECI for around one-tenth of the land surface. The highly affected areas mainly correspond to regions with high mountain ranges. For wind the majority of the land surface corresponds to ECIV. Still, around one-quarter of the land surface belongs to the high change categories (ECI and ECII).

3.8 Discussion of runoff sensitivities

Here we compare our findings to the respective literature to assess the realism of JULES' sensitivity. We use the median sensitivity value of the grid boxes of each region (Table 4) as the representative sensitivity S for each region. Moreover, we discuss issues of possible model over-sensitivity in particular regions and the caveats of this study.

3.8.1 Sensitivity of runoff to precipitation

Most studies have examined the sensitivity (also reported as elasticity) of runoff (or discharge) to precipitation. A number of studies have examined sensitivity to precipitation for regions or basins in the United States. Values of runoff sensi-

tivity (S) to precipitation between 1.5 and 2.5 were reported by Sankarasubramanian and Vogel (2003) for the US (WNA, CNA, and ENA). Fu et al. (2007) reported values of 1.5 to 1.67 for the Spokane River basin (located in WNA). Vano et al. (2012) found that S to precipitation ranged from 2.2 to 3.3 for different LSMs for the Colorado River basin (also located in WNA). For the Mississippi River basin (mainly located in CNA), Renner et al. (2012) found that S of streamflow to precipitation is 2.38 and 2.55 using two different methods for sensitivity estimation. For another basin located in CNA, Brikowski (2015) reported runoff S to precipitation to be 2.64. For the US region, the S values found in this study compare very well with the literature values. Runoff S to precipitation is 2.12 for WNA, 2.54 for CNA, and 1.69 for ENA. Many studies report S to precipitation for regions or basins of China. Reported values of runoff S to precipitation in the Yellow River basin (located in EAS) are 1.4 to 1.69 (Fu et al., 2007), 1.6 to 3.9 for 89 catchments of the EAS region (Yang and Yang, 2011), and 1.71 and 1.74 (estimates of two different methods) for the headwaters of the Yellow River (Renner et al., 2012). Again, the value found in our study is in good

Table 4. Relative change (%) in forcing variable (ΔV), corresponding relative change (%) in runoff (ΔRF), and sensitivities ($S = \Delta RF/\Delta V$) per region, for each variable. For each region, the median of the ΔV , ΔRF , and S values of all land grid boxes is shown.

	Variables	P	T^*	R	H	Ps	W
GLOBAL	ΔV	14.46	-0.57	1.73	0.91	-0.02	-5.86
	ΔRF	2.49	3.38	-3.71	2.04	-0.04	0.21
	S	1.76	-0.05	-2.12	0.81	1.18	-0.06
NEU	ΔV	14.6	-0.46	1.86	4.1	-0.05	-9.79
	ΔRF	27.97	22.68	-5.25	25.49	-0.02	3.62
	S	2.10	-0.31	-3.31	5.24	2.90	-0.36
MED	ΔV	-14.39	-0.15	0.55	-1.34	0.41	14.94
	ΔRF	-58.56	1.55	-1.51	4.07	0.44	-0.47
	S	2.02	-0.04	-2.52	0.77	1.08	-0.08
NEE	ΔV	4.89	-1.44	2.44	3.32	0.1	-11.77
	ΔRF	5.75	47.11	-5.39	32.73	0.26	5.98
	S	2.28	-0.32	-2.64	9.58	3.31	-0.50
NAS	ΔV	26.05	0.67	3.53	8.05	-0.06	-1.08
	ΔRF	59.36	11.8	-10.08	63.98	0.02	4.06
	S	2.35	-0.07	-2.95	7.58	2.43	-0.29
CAS	ΔV	6.44	-0.03	1.37	-13.00	-0.41	8.09
	ΔRF	-9.94	1.31	-0.44	-0.19	-0.36	-1.29
	S	2.49	-0.05	-3.50	0.31	0.88	-0.09
TIB	ΔV	128.47	-2.94	-1.14	7.69	-0.12	12.59
	ΔRF	1017.17	5.38	0.97	0.81	0.02	0.06
	S	7.27	-0.02	-2.07	0.18	0.40	0.00
EAS	ΔV	19.25	-0.94	2.51	2.92	-0.2	-3.55
	ΔRF	4.36	5.54	-2.96	3.66	-0.05	0.76
	S	1.70	-0.06	-1.53	0.82	1.07	-0.09
SEA	ΔV	19.76	-0.87	1.11	0.89	0.23	34.57
	ΔRF	43.92	5.97	-3.2	1.66	0.32	-1.04
	S	2.07	-0.08	-2.68	1.16	1.54	-0.05
NAU	ΔV	41.15	-0.04	1.43	7.71	0.1	-28.46
	ΔRF	-5.13	1.02	-1.16	1.38	0.09	-0.44
	S	0.37	-0.03	-0.75	0.31	0.56	0.00
SAU	ΔV	18.92	-0.28	0.85	2	-0.13	-11.2
	ΔRF	-9.29	1.07	-0.11	1.4	0.06	-0.49
	S	0.82	-0.05	-0.88	0.67	1.00	-0.03
SAH	ΔV	54.11	-2.73	-0.47	-8.96	0.22	-13.59
	ΔRF	-2.59	-0.68	0.64	-0.32	0	0.08
	S	0.94	0.00	-0.25	0.04	0.04	-0.01
WAF	ΔV	26.74	-1.51	-0.88	-5.79	-0.1	-15.13
	ΔRF	58.24	5.61	-1.57	-0.71	-0.13	0.09
	S	2.78	-0.04	-2.61	0.22	1.28	-0.04
EAF	ΔV	23.22	-1.68	-0.06	-5.76	-0.25	-12.11
	ΔRF	42.13	7.24	-1.51	-3.74	-0.28	0.09
	S	2.12	-0.05	-1.95	0.48	0.95	0.00
EQF	ΔV	5.64	-1.55	-0.25	-2.15	-0.2	-10.09
	ΔRF	-0.14	6.21	0.92	-1.29	0	0.07
	S	2.26	-0.05	-1.73	0.49	0.92	-0.01

Table 4. Continued.

	Variables	<i>P</i>	<i>T</i> *	<i>R</i>	<i>H</i>	Ps	<i>W</i>
SQF	ΔV	36.45	-0.9	0.9	0.89	-0.03	-15.6
	ΔRF	-73.18	-82.26	-85.07	-84.68	-84.2	-84.18
	<i>S</i>	2.94	-0.07	-1.91	0.59	1.10	-0.04
SAF	ΔV	89.8	-1.41	-0.38	14.28	0.68	-4.74
	ΔRF	85.47	5.5	0.54	5.33	0.42	-0.02
	<i>S</i>	1.35	-0.04	-1.66	0.45	0.72	-0.05
WNA	ΔV	65.92	-1.75	-1.23	13.55	0.14	10.23
	ΔRF	112.66	17.94	-0.48	9.85	0.16	-2.5
	<i>S</i>	2.12	-0.13	-2.01	0.77	0.98	-0.17
CNA	ΔV	-12.84	0.11	1.68	2.29	-0.08	-14.79
	ΔRF	-50.86	1.53	-2.06	6.57	-0.05	1.96
	<i>S</i>	2.54	-0.07	-1.47	1.08	1.09	-0.13
ENA	ΔV	4.08	0.49	2.71	13.4	0.1	5.47
	ΔRF	-0.38	-0.38	-5.18	39.72	0.13	0.86
	<i>S</i>	1.69	-0.07	-1.92	3.17	1.54	-0.11
CAM	ΔV	11.43	-0.98	-0.4	-6.16	0.15	25.27
	ΔRF	-7.73	3.65	-0.1	-2.55	0.14	-0.52
	<i>S</i>	1.32	-0.04	-1.58	0.49	0.77	-0.02
AMZ	ΔV	-26.58	-0.35	4.06	-13.19	-0.19	-4
	ΔRF	-40.52	4.88	-9.34	-6.01	-0.23	0.03
	<i>S</i>	1.42	-0.05	-2.37	0.53	1.44	-0.04
CSA	ΔV	-32.8	0.7	3.05	-11.53	-0.23	-7.5
	ΔRF	-63.21	-1.49	-3.22	-5.75	-0.13	0.38
	<i>S</i>	1.59	-0.04	-1.16	0.53	0.83	-0.04
SSA	ΔV	72.07	-1.22	-1.77	5.07	0.08	9.91
	ΔRF	84.32	10.06	-0.47	12.05	0.34	-2.44
	<i>S</i>	1.53	-0.09	-0.50	1.48	1.29	-0.04
SAS	ΔV	-9.19	-1.08	1.39	-13.11	-0.05	-6.81
	ΔRF	-26.35	5.2	-4.07	-2.53	-0.09	0.51
	<i>S</i>	1.62	-0.05	-2.46	0.29	0.90	-0.05

* ΔV for temperature is the absolute change in temperature.

Table 5. Percent of land area (%) under each of the four effect categories (ECs).

Variables/ ECs	I	II	III	IV
<i>P</i>	67.80	24.20	1.82	6.18
<i>T</i>	45.15	22.03	2.46	30.35
<i>R</i>	48.74	1.30	26.16	23.80
<i>H</i>	40.80	13.76	5.58	39.86
Ps	12.17	1.83	38.48	47.52
<i>W</i>	6.09	19.19	2.35	72.37

agreement with the literature (*S* to precipitation for EAS is 1.70).

3.8.2 Sensitivity of runoff to temperature and other variables

A number of studies have examined runoff sensitivity to temperature changes. Vano et al. (2012) reported *S* to temperature values ranging from -2 to -9C^{-1} between five LSMs for the Colorado River basin (WNA) and Brikowski (2015) reported a value of -0.41C^{-1} for *S* to temperature in a basin in CNA. Our values for these regions are substantially lower (-0.13K^{-1} for WNA and -0.07K^{-1} for CNA). This divergence could be attributed to two factors. First, to an extent it could be connected to possible non-sensitivities of our model to temperature changes for these regions. Second, the differences could arise from the inclusion (or not) of the physical link between temperature and other variables in the analysis. Vano et al. (2012) use different LSMs to calculate sensitiv-

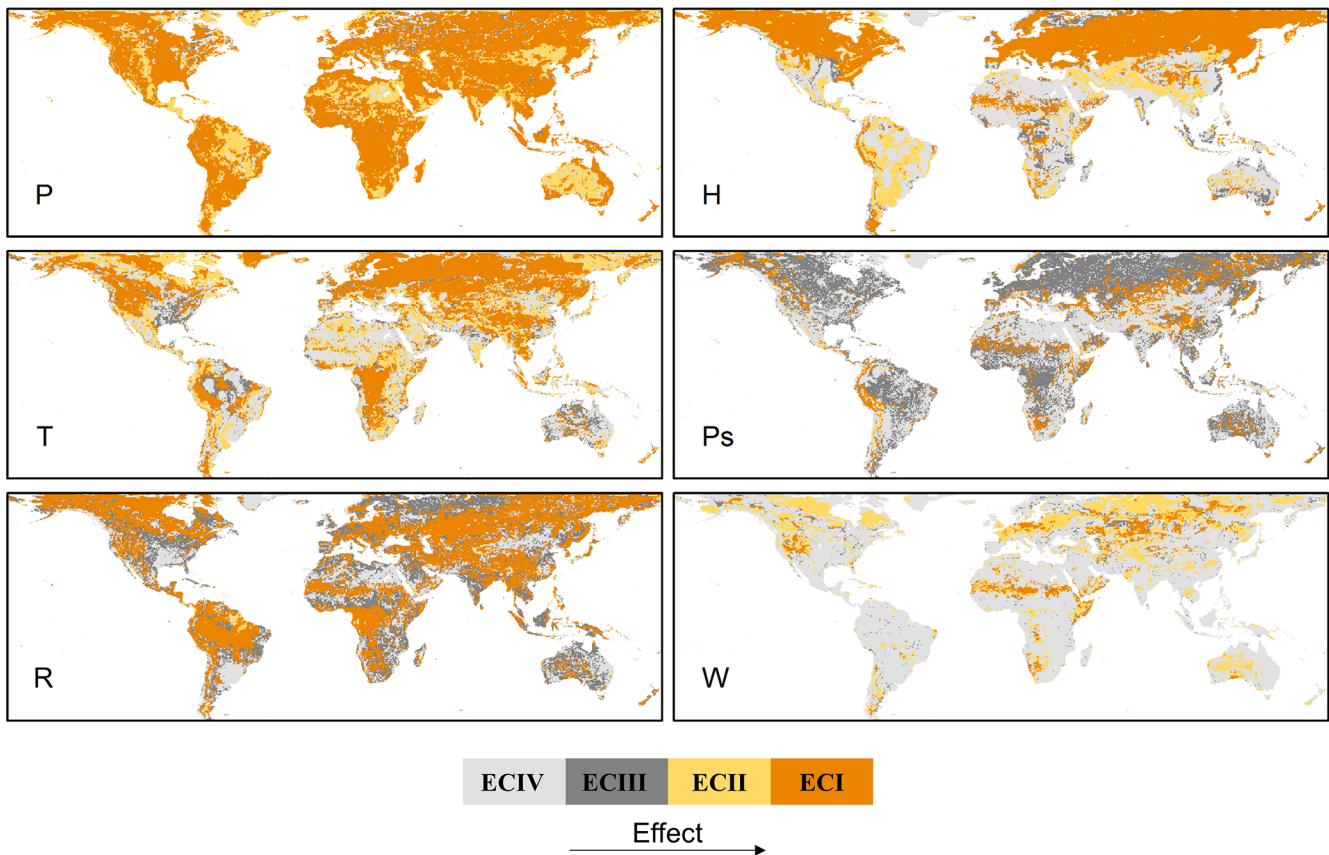


Figure 10. Global maps of bias effect categories (ECs) for each forcing variable.

ities by perturbing daily temperature maxima and minima. These changes also affect the downward longwave radiation and humidity, which are then used by the evapotranspiration routines of the LSMs. In our case, the change in temperature does not interact with radiation and humidity, as those are read as input variables by the model. When temperature is allowed to interact with humidity, increased temperature will increase the water vapour capacity of the air, and more water will be evaporated. The lack of this physical link in our simulations could, to an extent, explain the decreased sensitivity of runoff to temperature changes compared to Vano et al. (2012). In the analysis of Brikowski (2015), sensitivities of runoff to precipitation and temperature are derived from the respective historical data. Thus, sensitivity to temperature will also include the changes caused by the interaction of temperature with other meteorological variables. In a study with a different approach, Yang and Yang (2011) separated the effect of precipitation, temperature, net radiation, relative humidity, and wind speed on runoff and calculated sensitivities for each variable. They reported values of S to temperature ranging from -0.11 to -0.02 C^{-1} between 89 catchments of the EAS region. For the same region, we have computed S to temperature as -0.06 K^{-1} , which is included in the stated range in the literature. Moreover, our S val-

ues for radiation, humidity, and wind speed are also in good agreement with Yang and Yang (2011). According to Yang and Yang (2011), S to radiation ranges from -1.9 to -0.3 , S to humidity from 0.2 to 1.9 , and S to wind speed from -0.8 to -0.1 . The range refers to values computed for 89 catchments in the EAS region. Our respective values for this region are -1.53 for radiation, 0.82 for humidity, and -0.09 for wind speed. This supports the argument that the large deviations of the sensitivity to temperature between our study and the studies of Vano et al. (2012) and Brikowski (2015) result from interactions in the forcing variables included in the referenced studies.

3.8.3 Sensitivity of runoff to radiation

The reported S to radiation values are higher in absolute terms than S to precipitation values for many of the examined regions and also globally (Table 4). However, according to the findings presented in Sect. 3.5, precipitation and temperature correspond to higher changes in runoff compared to radiation. That is because high S to radiation results from relatively low ΔV values, rather than from relatively high ΔRF values (compared e.g. to precipitation). Small ΔV for radiation is possibly the consequence of combining shortwave and longwave radiation to calculate the total bias in radiation, as

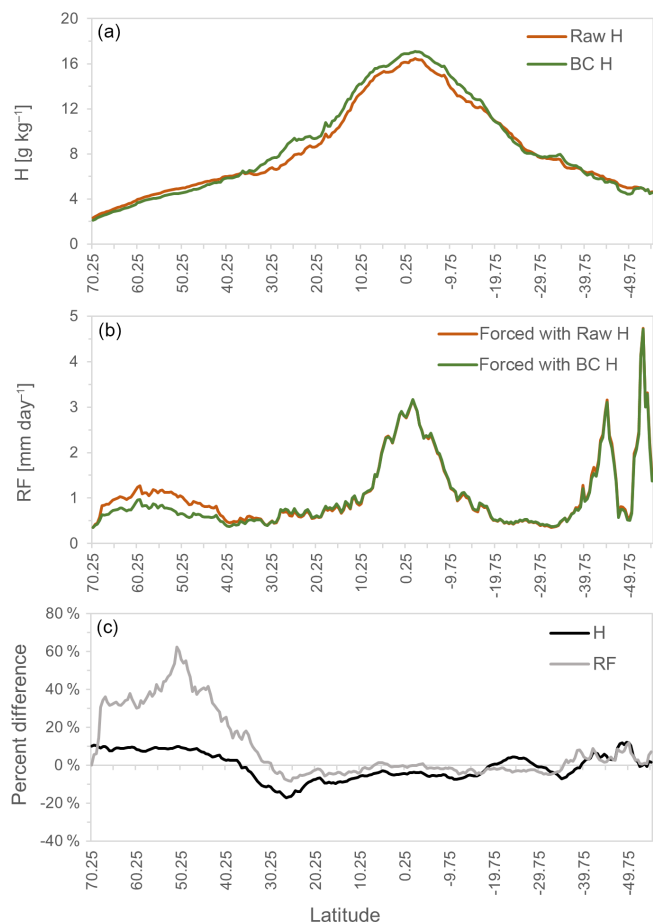


Figure 11. (a) Latitudinal means of raw and bias corrected specific humidity (g kg^{-1}), (b) latitudinal means of JULES' runoff forced with raw and bias corrected specific humidity (mm day^{-1}), and (c) percent differences of the latitudinal means in (a) H and (b) RF . The latitudinal means are calculated from the 1981–2010 period.

the two radiation components have inverse signs for most regions (Fig. 5).

3.8.4 Sensitivity of runoff to specific humidity in high-latitude regions

Although S to humidity for EAS compares well with the literature, unexpectedly high values of S to humidity are found for other regions (5.24 for NEU, 9.58 for NEE, and 7.58 for NAS). We performed an extra analysis to investigate this issue and the basic findings are included in Fig. 11 and the Supplement of this paper. Figure 11 examines the differences between the latitudinal mean of raw and bias corrected specific humidity and the resulting runoff. Very high sensitivity of runoff to H is observed for a specific area, the zone between 70 and 40° N latitudes. In that zone, a difference of about 10% in H corresponds to an increase of 40 to 60% in runoff. Investigation of the different fluxes related to runoff production in the model revealed two mechanisms

that explain this behaviour. First, due to higher humidity, the water vapour deficit of the air is reduced and evapotranspiration is decreased, thus allowing more of the precipitated water available as runoff. This mechanism explains around one-third of the magnitude of reported changes in runoff (Fig. S4). The second mechanism happens due to supersaturation of the air, especially during the colder months of the year when the dew point is lower, and includes the condensation and deposition of water vapour (direct transition from vapour to ice). Deposited water accumulates as snow mass. Snow mass is higher for the raw H run (H has positive biases), which results in increased snowmelt and thus increased runoff (Fig. S5).

A comparison of supersaturated air conditions for the different sets of data (WFDEI, raw, BC, and NobcH) can help us identify the origin of the aforementioned behaviour. From the input specific humidity H , we estimated the respective relative humidity (this transformation also requires temperature T and surface pressure P_s as input to the Clausius–Clapeyron equation). Then we calculated the fraction of time (based on a daily time step) in which supersaturated conditions occur, for the historical period 1981–2010. The estimation was performed for (a) the WFDEI H , T , and P_s , (b) the raw H , T , and P_s , (c) the bias corrected H , T , and P_s , and (d) for a combination of data corresponding to the NobcH run (raw H combined with bias corrected T and P_s). The results are presented in Fig. 6 of the Supplement of this paper. The analysis reveals that the higher-latitude regions – that display high sensitivity of runoff to H – are under supersaturated conditions for more than 10% of the time (Fig. S6). The length of supersaturated conditions estimated for the WFDEI, raw, or BC data do not exhibit a respective spatial pattern, although supersaturation is found in all three datasets (Fig. S6). Thus, the high runoff sensitivity over the high-latitude regions is not a result of supersaturated conditions in the raw GCM H , and it rather stems from (1) raw GCM H being higher than BC H and (2) the calculation of relative humidity within JULES, done by combining raw GCM H with bias corrected T and P_s . This inconsistency strengthens the argument for the need for bias correction of more forcing variables – in addition to P and T . Specific humidity is a variable that is often left uncorrected, a practice that could possibly result in runoff overestimations at the northern latitudes based on our findings, in cases where hydrological models which account for deposition and condensation are used.

Since this experiment was performed with a single LSM, it cannot be concluded whether this behaviour is common between the LSMs or is an over-sensitivity of the JULES model. However, it highlights the importance of bias correction for specific humidity for specific regions, where runoff would have been highly overestimated using raw specific humidity as forcing.

3.9 Study caveats

An issue that must be considered for the interpretation of the results of this study is that they have been based on a single impact model. As the uncertainty stemming from the selection of the impact model is large (Gudmundsson et al., 2012; Hagemann et al., 2013), it is preferable to use multiple models in order to capture a wide range of possible results. The effect of the meteorological forcing on a hydrological output is heavily model dependent, as different models employ different concepts and/or equations for the representation of key hydrological processes. This concern has also been discussed by other single model studies on meteorological variables' effects on hydrological outputs (Mizukami et al., 2014; Masaki et al., 2015). Nonetheless, the results of single model studies are useful in giving indicative answers on the issues they examine and set a basis for the methodology needed for the respective multi-model applications.

4 Summary and conclusions

The present study examined the effect of the biases in GCM output variables on historical runoff simulations, using the JULES LSM. The effects of biases were studied for each forcing variable separately, for a total of six meteorological variables (precipitation, temperature, radiation, specific humidity, surface pressure, and wind speed). Biases of each variable and the respective effect of runoff were quantified at the global and regional scales. A framework for the categorization of the effects of biases of the different variables was developed and implemented, leading to global maps of bias ECs.

We found that bias correction of GCM outputs results in substantially improved representation of historical runoff. For this reason, our study adds to the numerous studies that advocate the use of some kind of bias correction of GCM data prior to their use as impact model forcing. Precipitation and temperature biases were identified as causing the largest changes in runoff. Radiation and specific humidity can also have a substantial effect on runoff, especially for specific regions. The sensitivity of runoff to the different forcing variables exhibits a high spatial variability. Depending on the region, runoff can be more sensitive to radiation or humidity compared to precipitation or temperature. The produced EC maps show that all variables can potentially affect runoff to a high extent, depending on the region. The fraction of the land surface occupied by the high effect category ECI (high changes in runoff and high sensitivity of runoff to the variable's changes) ranges between the variables from 67.80 % for precipitation to 6.09 % for wind.

The produced maps of ECs aid the identification of the regions most affected by the bias of each variable. Thus, they could serve as a decision tool in cases when an informed decision needs to be made on the variables that would need to

be bias corrected or could be neglected from bias correction, according to the planned model application. Moreover, when raw forcing is used in model applications, EC maps could provide guidance towards the areas where the results would need more careful interpretation.

Based on the findings of this study, we suggest that the widely used concept of bias correcting precipitation and temperature should be extended to include more input variables. Radiation and specific humidity should be added to the priority variables for bias correction in hydrological applications, along with precipitation and temperature.

Due to the heavily model-dependent nature of runoff sensitivity to forcing variables, generalized conclusions for the behaviour of other impact models to GCM biases cannot be drawn from the present single model assessment. Nevertheless, this study aims to initiate a discussion of the effect of GCM biases on hydrological output, as the consideration of these sensitivities is crucial to understanding the uncertainty spectrum of hydrologically relevant climate change assessments.

Data availability. The WFDEI.GPCC datasets treated as observations in the present study were provided in the framework of the ISIMIP project (<http://www.isimip.org/>) and obtained through the vre2.dkrz.de server. Raw climate model data (IPSL-CM5A, MIROC-ESM-CHEM, GFDL-ESM2M) of the CMIP5 project have been downloaded through the Earth System Grid Federation (ESGF) (<https://esgf-node.llnl.gov/search/cmip5/>).

The Supplement related to this article is available online at <https://doi.org/10.5194/hess-21-4379-2017-supplement>.

Competing interests. The authors declare that they have no conflict of interest.

Acknowledgements. We acknowledge the World Climate Research Programme's Working Group on Coupled Modelling, which is responsible for CMIP, and we thank the climate modelling groups (listed in Table 1 of this paper) for producing and making available their model output. For CMIP the US Department of Energy's Program for Climate Model Diagnosis and Intercomparison provides coordinating support and led development of software infrastructure in partnership with the Global Organization for Earth System Science Portals.

The research leading to these results has received funding from the HELIX project of the European Union's Seventh Framework Programme for research, technological development and demonstration under grant agreement no. 603864.

Edited by: Stacey Archfield

Reviewed by: two anonymous referees

References

- Best, M. J., Pryor, M., Clark, D. B., Rooney, G. G., Essery, R. L. H., Ménard, C. B., Edwards, J. M., Hendry, M. A., Porson, A., Gedney, N., Mercado, L. M., Sitch, S., Blyth, E., Boucher, O., Cox, P. M., Grimmond, C. S. B., and Harding, R. J.: The Joint UK Land Environment Simulator (JULES), model description – Part 1: Energy and water fluxes, *Geosci. Model Dev.*, 4, 677–699, <https://doi.org/10.5194/gmd-4-677-2011>, 2011.
- Blyth, E., Clark, D. B., Ellis, R., Huntingford, C., Los, S., Pryor, M., Best, M., and Sitch, S.: A comprehensive set of benchmark tests for a land surface model of simultaneous fluxes of water and carbon at both the global and seasonal scale, *Geosci. Model Dev.*, 4, 255–269, <https://doi.org/10.5194/gmd-4-255-2011>, 2011.
- Brikowski, T. H.: Applying multi-parameter runoff elasticity to assess water availability in a changing climate: An example from Texas, USA, *Hydrol. Process.*, 29, 1746–1756, <https://doi.org/10.1002/hyp.10297>, 2015.
- Bromwich, D. H., Otieno, F. O., Hines, K. M., Manning, K. W., and Shilo, E.: Comprehensive evaluation of polar weather research and forecasting model performance in the Antarctic, *J. Geophys. Res.-Atmos.*, 118, 274–292, <https://doi.org/10.1029/2012JD018139>, 2013.
- Christensen, J. H., Boberg, F., Christensen, O. B., and Lucas-Picher, P.: On the need for bias correction of regional climate change projections of temperature and precipitation, *Geophys. Res. Lett.*, 35, L20709, <https://doi.org/10.1029/2008GL035694>, 2008.
- Clark, D. B., Mercado, L. M., Sitch, S., Jones, C. D., Gedney, N., Best, M. J., Pryor, M., Rooney, G. G., Essery, R. L. H., Blyth, E., Boucher, O., Harding, R. J., Huntingford, C., and Cox, P. M.: The Joint UK Land Environment Simulator (JULES), model description – Part 2: Carbon fluxes and vegetation dynamics, *Geosci. Model Dev.*, 4, 701–722, <https://doi.org/10.5194/gmd-4-701-2011>, 2011.
- Coxon, G., Freer, J., Westerberg, I. K., Wagener, T., Woods, R., and Smith, P. J.: A novel framework for discharge uncertainty quantification applied to 500 UK gauging stations, *Water Resour. Res.*, 51, 5531–5546, <https://doi.org/10.1002/2014WR016532>, 2015.
- Demory, M. E., Vidale, P. L., Roberts, M. J., Berrisford, P., Strachan, J., Schiemann, R., and Mizielinski, M. S.: The role of horizontal resolution in simulating drivers of the global hydrological cycle, *Clim. Dynam.*, 42, 2201–2225, <https://doi.org/10.1007/s00382-013-1924-4>, 2014.
- Dufresne, J.-L., Foujols, M.-A., Denvil, S., Caubel, A., Marti, O., Aumont, O., Balkanski, Y., Bekki, S., Bellenger, H., Benshila, R., Bony, S., Bopp, L., Braconnot, P., Brockmann, P., Cadule, P., Cheruy, F., Codron, F., Cozic, A., Cugnet, D., de Noblet, N., Duvel, J.-P., Ethé, C., Fairhead, L., Fichet, T., Flavoni, S., Friedlingstein, P., Grandpeix, J.-Y., Guez, L., Guilyardi, E., Hauglustaine, D., Hourdin, F., Idelkadi, A., Ghattas, J., Jousaume, S., Kageyama, M., Krinner, G., Labetoulle, S., Lahellec, A., Lefebvre, M.-P., Lefebvre, F., Levy, C., Li, Z. X., Lloyd, J., Lott, F., Madec, G., Mancip, M., Marchand, M., Masson, S., Meurdesoif, Y., Mignot, J., Musat, I., Parouty, S., Polcher, J., Rio, C., Schulz, M., Swingedouw, D., Szopa, S., Talandier, C., Terray, P., Viovy, N., and Vuichard, N.: Climate change projections using the IPSL-CM5 Earth System Model: from CMIP3 to CMIP5, *Clim. Dynam.*, 40, 2123–2165, <https://doi.org/10.1007/s00382-012-1636-1>, 2013.
- Dunne, J. P., John, J. G., Adcroft, A. J., Griffies, S. M., Hallberg, R. W., Shevliakova, E., Stouffer, R. J., Cooke, W., Dunne, K. A., Harrison, M. J., Krasting, J. P., Malyshev, S. L., Milly, P. C. D., Phillippis, P. J., Sentman, L. T., Samuels, B. L., Spelman, M. J., Winton, M., Wittenberg, A. T., and Zadeh, N.: GFDL's ESM2 Global Coupled Climate–Carbon Earth System Models. Part I: Physical Formulation and Baseline Simulation Characteristics, *J. Climate*, 25, 6646–6665, <https://doi.org/10.1175/JCLI-D-11-00560.1>, 2012.
- Ehret, U., Zehe, E., Wulfmeyer, V., Warrach-Sagi, K., and Liebert, J.: HESS Opinions “Should we apply bias correction to global and regional climate model data?”, *Hydrol. Earth Syst. Sci.*, 16, 3391–3404, <https://doi.org/10.5194/hess-16-3391-2012>, 2012.
- Elsner, M. M., Gangopadhyay, S., Pruitt, T., Brekke, L. D., Mizukami, N., Clark, M. P., Elsner, M. M., Gangopadhyay, S., Pruitt, T., Brekke, L. D., Mizukami, N., and Clark, M. P.: How Does the Choice of Distributed Meteorological Data Affect Hydrologic Model Calibration and Streamflow Simulations?, *J. Hydrometeorol.*, 15, 1384–1403, <https://doi.org/10.1175/JHM-D-13-083.1>, 2014.
- Fu, G., Charles, S. P., and Chiew, F. H. S.: A two-parameter climate elasticity of streamflow index to assess climate change effects on annual streamflow, *Water Resour. Res.*, 43, 1–12, <https://doi.org/10.1029/2007WR005890>, 2007.
- Giorgi, F. and Bi, X.: Updated regional precipitation and temperature changes for the 21st century from ensembles of recent AOGCM simulations, *Geophys. Res. Lett.*, 32, L21715, <https://doi.org/10.1029/2005GL024288>, 2005.
- Grillakis, M. G., Koutroulis, A. G., and Tsanis, I. K.: Multisegment statistical bias correction of daily GCM precipitation output, *J. Geophys. Res.-Atmos.*, 118, 3150–3162, <https://doi.org/10.1002/jgrd.50323>, 2013.
- Grillakis, M. G., Koutroulis, A. G., Papadimitriou, L. V., Daliakopoulos, I. N., and Tsanis, I. K.: Climate-Induced Shifts in Global Soil Temperature Regimes, *Soil Sci.*, 181, 264–272, 2016.
- Grillakis, M. G., Koutroulis, A. G., Daliakopoulos, I. N., and Tsanis, I. K.: A method to preserve trends in quantile mapping bias correction of climate modeled temperature, *Earth Syst. Dynam. Discuss.*, <https://doi.org/10.5194/esd-2017-53>, in review, 2017.
- Gudmundsson, L., Tallaksen, L. M., Stahl, K., Clark, D. B., Dumont, E., Hagemann, S., Bertrand, N., Gerten, D., Heinke, J., Hanasaki, N., and Voss, F.: Comparing large-scale hydrological model simulations to observed runoff percentiles in Europe, *J. Hydrometeorol.*, 13, 604–620, 2012.
- Haddeland, I., Heinke, J., Voß, F., Eisner, S., Chen, C., Hagemann, S., and Ludwig, F.: Effects of climate model radiation, humidity and wind estimates on hydrological simulations, *Hydrol. Earth Syst. Sci.*, 16, 305–318, <https://doi.org/10.5194/hess-16-305-2012>, 2012.
- Hagemann, S., Chen, C., Haerter, J. O., Heinke, J., Gerten, D., and Piani, C.: Impact of a Statistical Bias Correction on the Projected Hydrological Changes Obtained from Three GCMs and Two Hydrology Models, *J. Hydrometeorol.*, 12, 556–578, <https://doi.org/10.1175/2011JHM1336.1>, 2011.
- Hagemann, S., Chen, C., Clark, D. B., Folwell, S., Gosling, S. N., Haddeland, I., Hanasaki, N., Heinke, J., Ludwig, F.,

- Voss, F., and Wiltshire, A. J.: Climate change impact on available water resources obtained using multiple global climate and hydrology models, *Earth Syst. Dynam.*, 4, 129–144, <https://doi.org/10.5194/esd-4-129-2013>, 2013.
- Hansen, J. W., Challinor, A., Ines, A. V. M., Wheeler, T., and Moron, V.: Translating climate forecasts into agricultural terms: advances and challenges, *Clim. Res.*, 33, 27–41, 2006.
- Harding, R. J., Weedon, G. P., van Lanen, H. A. J., and Clark, D. B.: The future for Global Water Assessment, *J. Hydrol.*, 518, 186–193, <https://doi.org/10.1016/j.jhydrol.2014.05.014>, 2014.
- Haslinger, K., Anders, I., and Hofstätter, M.: Regional climate modelling over complex terrain: an evaluation study of COSMO-CLM hindcast model runs for the Greater Alpine Region, *Clim. Dynam.*, 40, 511–529, <https://doi.org/10.1007/s00382-012-1452-7>, 2013.
- Hattermann, F., Krysanova, V., Gosling, S. N., Dankers, R., Daggupati, P., Donnelly, C., Flörke, M., Huang, S., Motovilov, Y., Buda, S., Yang, T., Muller, C., Leng, G., Tang, Q., Portmann, F. T., Hagemann, S., Gerten, D., Wada, Y., Masaki, Y., Alemayehu, T., Satoh, Y., and Samaniego, L.: Cross-scale intercomparison of climate change impacts simulated by regional and global hydrological models in eleven large river basins, *Climatic Change*, 141, 561–576, <https://doi.org/10.1007/s10584-016-1829-4>, 2017.
- Katzav, J. and Parker, W. S.: The future of climate modeling, *Climatic Change*, 132, 475–487, <https://doi.org/10.1007/s10584-015-1435-x>, 2015.
- King, A. D., Donat, M. G., Fischer, E. M., Hawkins, E., Alexander, L. V., Karoly, D. J., Dittus, A. J., Lewis, S. C., and Perkins, S. E.: The timing of anthropogenic emergence in simulated climate extremes, *Environ. Res. Lett.*, 10, 94015, <https://doi.org/10.1088/1748-9326/10/9/094015>, 2015.
- Koutroulis, A. G., Grillakis, M. G., Tsanis, I. K., and Papadimitriou, L.: Evaluation of precipitation and temperature simulation performance of the CMIP3 and CMIP5 historical experiments, *Clim. Dynam.*, 47, 1881–1898, <https://doi.org/10.1007/s00382-015-2938-x>, 2016.
- Li, H., Sheffield, J., and Wood, E. F.: Bias correction of monthly precipitation and temperature fields from Intergovernmental Panel on Climate Change AR4 models using equidistant quantile matching, *J. Geophys. Res.*, 115, D10101, <https://doi.org/10.1029/2009JD012882>, 2010.
- Maraun, D.: Nonstationarities of regional climate model biases in European seasonal mean temperature and precipitation sums, *Geophys. Res. Lett.*, 39, L06706, <https://doi.org/10.1029/2012GL051210>, 2012.
- Maraun, D., Wetterhall, F., Ireson, A. M., Chandler, R. E., Kendon, E. J., Widmann, M., Brienen, S., Rust, H. W., Sauter, T., Thiemel, M., Venema, V. K. C., Chun, K. P., Goodess, C. M., Jones, R. G., Onof, C., Vrac, M., and Thiele-Eich, I.: Precipitation downscaling under climate change: Recent developments to bridge the gap between dynamical models and the end user, *Rev. Geophys.*, 48, RG3003, <https://doi.org/10.1029/2009RG000314>, 2010.
- Masaki, Y., Hanasaki, N., Takahashi, K., and Hijikawa, Y.: Propagation of biases in humidity in the estimation of global irrigation water, *Earth Syst. Dynam.*, 6, 461–484, <https://doi.org/10.5194/esd-6-461-2015>, 2015.
- Miao, C., Su, L., Sun, Q., and Duan, Q.: A nonstationary bias-correction technique to remove bias in GCM simulations, *J. Geophys. Res.-Atmos.*, 121, 5718–5735, <https://doi.org/10.1002/2015JD024159>, 2016.
- Mizukami, N., Clark, M. P., Slater, A. G., Brekke, L. D., Elsner, M. M., Arnold, J. R., and Gangopadhyay, S.: Hydrologic Implications of Different Large-Scale Meteorological Model Forcing Datasets in Mountainous Regions, *J. Hydrometeorol.*, 15, 474–488, <https://doi.org/10.1175/JHM-D-13-036.1>, 2014.
- Monteith, J. L.: Evaporation and environment. The state and movement of water in living organisms, *Symposium of the society of experimental biology*, Vol. 19, 205–234, 1965.
- Müller Schmied, H., Eisner, S., Franz, D., Wattenbach, M., Portmann, F. T., Flörke, M., and Döll, P.: Sensitivity of simulated global-scale freshwater fluxes and storages to input data, hydrological model structure, human water use and calibration, *Hydrol. Earth Syst. Sci.*, 18, 3511–3538, <https://doi.org/10.5194/hess-18-3511-2014>, 2014.
- Nikulin, G., Bosshard, T., Yang, W., Barring, L., Wilcke, R., Vrac, M., Vautard, R., Noel, T., Gutiérrez, J. M., Herrera, S., Fernández, J., Haugen, J. E., Benestad, R., Landgren, O. A., Grillakis, M., Tsanis, I., Koutroulis, A., Dosio, A., Ferrone, A., and Switanek, M.: Bias Correction Intercomparison Project (BCIP): an introduction and the first results, in *EGU General Assembly Conference Abstracts*, p. 2250, 2015.
- Oki, T. and Sud, Y. C.: Design of Total Runoff Integrating Pathways (TRIP) – A Global River Channel Network, 2, 7–22, 1998.
- O’Neill, B. C., Oppenheimer, M., Warren, R., Hallegatte, S., Kopp, R. E., Pörtner, H. O., Scholes, R., Birkmann, J., Foden, W., Licker, R., Mach, K. J., Marbaix, P., Mastrandrea, M. D., Price, J., Takahashi, K., van Ypersele, J.-P., and Yohe, G.: IPCC reasons for concern regarding climate change risks, *Nat. Publ. Gr.*, 7, 28–37, <https://doi.org/10.1038/NCLIMATE3179>, 2017.
- Papadimitriou, L. V., Koutroulis, A. G., Grillakis, M. G., and Tsanis, I. K.: High-end climate change impact on European runoff and low flows – exploring the effects of forcing biases, *Hydrol. Earth Syst. Sci.*, 20, 1785–1808, <https://doi.org/10.5194/hess-20-1785-2016>, 2016.
- Photiadou, C., van den Hurk, B., van Delden, A., and Weerts, A.: Incorporating circulation statistics in bias correction of GCM ensembles: hydrological application for the Rhine basin, *Clim. Dynam.*, 46, 187–203, <https://doi.org/10.1007/s00382-015-2578-1>, 2016.
- Piani, C., Weedon, G. P., Best, M., Gomes, S. M., Viterbo, P., Hagemann, S., and Haerter, J. O.: Statistical bias correction of global simulated daily precipitation and temperature for the application of hydrological models, *J. Hydrol.*, 395, 199–215, <https://doi.org/10.1016/j.jhydrol.2010.10.024>, 2010.
- Randall, D. A., Wood, R. A., Bony, S., Colman, R., Fichet, T., Fyfe, J., Kattsov, V., Pitman, A., Shukla, J., Srinivasan, J., Stouffer, R. J., Sumi, A., and Tayler, K. E.: *Climate Models and Their Evaluation*, *Clim. Chang. 2007 Phys. Sci. Basis*, edited by: Solomon al., S., Qin, D., Manning, M., Chen, Z., Marquis, M., Averyt, K. B., Tignor, M., and Miller, H. L., Cambridge Univ. Press, 589–662, 2007.
- Renner, M., Seppelt, R., and Bernhofer, C.: Evaluation of water-energy balance frameworks to predict the sensitivity of streamflow to climate change, *Hydrol. Earth Syst. Sci.*, 16, 1419–1433, <https://doi.org/10.5194/hess-16-1419-2012>, 2012.
- Rojas, R., Feyen, L., Dosio, A., and Bavera, D.: Improving pan-European hydrological simulation of extreme events

- through statistical bias correction of RCM-driven climate simulations, *Hydrol. Earth Syst. Sci.*, 15, 2599–2620, <https://doi.org/10.5194/hess-15-2599-2011>, 2011.
- Sankarasubramanian, A. and Vogel, R. M.: Hydroclimatology of the continental United States, *Geophys. Res. Lett.*, 30, 1–4, <https://doi.org/10.1029/2002GL015937>, 2003.
- Sharma, D., Das Gupta, A., and Babel, M. S.: Spatial disaggregation of bias-corrected GCM precipitation for improved hydrologic simulation: Ping River Basin, Thailand, *Hydrol. Earth Syst. Sci.*, 11, 1373–1390, <https://doi.org/10.5194/hess-11-1373-2007>, 2007.
- Solman, S. A., Sanchez, E., Samuelsson, P., da Rocha, R. P., Li, L., Marengo, J., Pessacq, N. L., Remedio, A. R. C., Chou, S. C., Berbery, H., Le Treut, H., de Castro, M., and Jacob, D.: Evaluation of an ensemble of regional climate model simulations over South America driven by the ERA-Interim reanalysis: model performance and uncertainties, *Clim. Dynam.*, 41, 1139–1157, <https://doi.org/10.1007/s00382-013-1667-2>, 2013.
- Stocker, T., Qin, D., Plattner, G.-K., Tignor, M., Allen, S., Boschung, J., Nauels, A., Xia, Y., Bex, V., and Migley, P.: IPCC, 2013: Summary for Policymakers, in: *Climate Change 2013: The Physical Science Basis*, Contribution of Working Group I to the Fifth Assessment Report of the Intergovernmental Panel on Climate Change, Cambridge University Press, Cambridge, United Kingdom and New York, NY, USA, 2013.
- Taylor, K. E., Stouffer, R. J., and Meehl, G. A.: An Overview of CMIP5 and the Experiment Design, *B. Am. Meteorol. Soc.*, 93, 485–498, <https://doi.org/10.1175/BAMS-D-11-00094.1>, 2012.
- Teng, J., Potter, N. J., Chiew, F. H. S., Zhang, L., Wang, B., Vaze, J., and Evans, J. P.: How does bias correction of regional climate model precipitation affect modelled runoff?, *Hydrol. Earth Syst. Sci.*, 19, 711–728, <https://doi.org/10.5194/hess-19-711-2015>, 2015.
- Teutschbein, C. and Seibert, J.: Bias correction of regional climate model simulations for hydrological climate-change impact studies: Review and evaluation of different methods, *J. Hydrol.*, 456–457, 12–29, <https://doi.org/10.1016/j.jhydrol.2012.05.052>, 2012.
- Themeßl, M. J., Gobiet, A., and Heinrich, G.: Empirical-statistical downscaling and error correction of regional climate models and its impact on the climate change signal, *Climatic Change*, 112, 449–468, <https://doi.org/10.1007/s10584-011-0224-4>, 2012.
- Uppala, S. M., Kållberg, P. W., Simmons, A. J., Andrae, U., Bechtold, V. D. C., Fiorino, M., Gibson, J. K., Haseler, J., Hernandez, A., Kelly, G. A., Li, X., Onogi, K., Saarinen, S., Sokka, N., Allan, R. P., Andersson, E., Arpe, K., Balmaseda, M. A., Beljaars, A. C. M., Berg, L. Van De, Bidlot, J., Bormann, N., Caires, S., Chevallier, F., Dethof, A., Dragosavac, M., Fisher, M., Fuentes, M., Hagemann, S., Hólm, E., Hoskins, B. J., Isaksen, I., Janssen, P. A. E. M., Jenne, R., McNally, A. P., Mahfouf, J.-F., Morcrette, J.-J., Rayner, N. A., Saunders, R. W., Simon, P., Sterl, A., Trenberth, K. E., Untch, A., Vasiljevic, D., Viterbo, P., and Woollen, J.: The ERA-40 re-analysis, *Q. J. Roy. Meteor. Soc.*, 131, 2961–3012, <https://doi.org/10.1256/QJ.04.176>, 2005.
- Vano, J. A., Das, T., and Lettenmaier, D. P.: Hydrologic Sensitivities of Colorado River Runoff to Changes in Precipitation and Temperature, *J. Hydrometeorol.*, 13, 932–949, <https://doi.org/10.1175/JHM-D-11-069.1>, 2012.
- Watanabe, S., Hajima, T., Sudo, K., Nagashima, T., Takemura, T., Okajima, H., Nozawa, T., Kawase, H., Abe, M., Yokohata, T., Ise, T., Sato, H., Kato, E., Takata, K., Emori, S., and Kawamiya, M.: MIROC-ESM 2010: model description and basic results of CMIP5-20c3m experiments, *Geosci. Model Dev.*, 4, 845–872, <https://doi.org/10.5194/gmd-4-845-2011>, 2011.
- Weedon, G. P., Gomes, S., Viterbo, P., Österle, H., Adam, J. C., Bellouin, N., Boucher, O., and Best, M.: The WATCH forcing data 1958–2001: A meteorological forcing dataset for land surface and hydrological models, *Watch. Ed. Watch Tech. Rep.*, 22, 2010.
- Weedon, G. P., Balsamo, G., Bellouin, N., Gomes, S., Best, M. J., and Viterbo, P.: The WFDEI meteorological forcing data set: WATCH Forcing Data methodology applied to ERA-Interim reanalysis data, *Water Resour. Res.*, 50, 7505–7514, <https://doi.org/10.1002/2014WR015638>, 2014.
- Yang, H. and Yang, D.: Derivation of climate elasticity of runoff to assess the effects of climate change on annual runoff, *Water Resour. Res.*, 47, 1–12, <https://doi.org/10.1029/2010WR009287>, 2011.
- Zulkafli, Z., Buytaert, W., Onof, C., Lavado, W., and Guyot, J. L.: A critical assessment of the JULES land surface model hydrology for humid tropical environments, *Hydrol. Earth Syst. Sci.*, 17, 1113–1132, <https://doi.org/10.5194/hess-17-1113-2013>, 2013.